

SLIM at LHC: LHC search power for a model linking dark matter and neutrino mass

Y. Farzan

*School of physics, Institute for Research in Fundamental Sciences (IPM), P.O. Box 19395-5531, Tehran, IRAN**

M. Hashemi

School of particles and accelerators, Institute for Research in Fundamental Sciences (IPM), P.O. Box 19395-5746, Tehran, IRAN

Recently a model has been proposed that links dark matter and neutrino masses. The dark matter candidate which is dubbed as SLIM has a mass of MeV scale and can show up at low energy experiments. The model also has a high energy sector which consists of a scalar doublet, (ϕ^-, ϕ^0) . We discuss the potential of the LHC for discovering the new scalars. We focus on the $\phi^+\phi^-$ and $\phi^\pm\phi^0$ production and the subsequent decay of the charged scalar to a charged lepton and the SLIM which appears as missing energy. Identifying the background, we estimate the signal significance and find that it can exceed 5σ at 30 fb^{-1} for the 14 TeV run at the LHC. We comment on the possibility of extracting the flavor structure of the Yukawa couplings which also determine the neutrino mass matrix. Finally, we discuss the prospects of this search at the current 7 TeV run of the LHC.

I. INTRODUCTION

The nature of dark matter and tiny but nonzero values of neutrino masses are two unsolved mysteries in particle physics and cosmology in early 21st century. Various models have been developed that explain nonzero neutrino masses. Rich literature also exists on the models suggesting a dark model candidate. Attempts to link these two mysteries and to solve them within a unique framework have only recently been started. In particular, in Ref. [1] a simple low energy scenario has been introduced which explains both phenomena in a minimalistic way. The scenario adds a real scalar which plays the role of the dark matter as well as two (or more) right-handed Majorana neutrinos that along with the scalar couple to the left-handed neutrinos. Through this Yukawa coupling, the left-handed neutrinos acquire a small Majorana mass at one-loop level. A Z_2 symmetry under which all new particles are odd is imposed to guarantee the stability of the lightest new particle which plays the role of the dark matter and is dubbed as SLIM. The Z_2 symmetry forbids a Dirac mass term for neutrinos. Within this scenario the main annihilation mode for dark matter is to (anti-)neutrino pairs. To simultaneously satisfy upper bound on the neutrino masses and to account for the observed dark matter abundance within thermal scenario (*i.e.*, $\langle\sigma(\text{DM} + \text{DM} \rightarrow \text{anything})v\rangle \simeq 3 \cdot 10^{-26} \text{ cm}^3/\text{sec}$), at least one of the right-handed neutrinos as well as the scalar have to be lighter than 10 MeV. On the other hand, these conditions lead to a lower bound on the couplings which makes the scenario testable in low energy experiments such as the measurement of $\text{Br}(\pi, K \rightarrow l_\alpha + \text{missing energy})$ [2].

With this minimal content, the new Yukawa coupling is not invariant under the electroweak symmetry so the low energy effective scenario has to be embedded in a $\text{SU}(3) \times \text{SU}(2) \times \text{U}(1)$ invariant model at higher energies. An example of such a model is introduced in [3]. The model includes a scalar electroweak doublet which has Yukawa couplings with charged leptons and the right-handed neutrinos. Like in the case of scenario [1], this Yukawa coupling gives rise to the neutrino masses at one-loop level. The model inherits the testability at low energy experiments from the low energy scenario that has been embedded in it. In addition, observable effects are expected in high energy experiments such as the LHC as well as in searches for lepton flavor violating decays such as $\mu \rightarrow e\gamma$. If the masses of the components of the electroweak doublet are not too high, these scalar particles can be produced through electroweak interactions at the LHC. As indicated in Ref. [3], it is in principle possible to derive the flavor structure of the Yukawa couplings at the LHC and compare it with the flavor structure deduced from the neutrino mass matrix.

In the present paper, we elaborate on this idea in detail. Considering various backgrounds and by employing state-of-the-art techniques for reconstructing the signal, the possibility of discovering the new particles is studied. We then discuss and propose conditions under which the Yukawa couplings can be derived. Several packages are linked together to ensure a reasonable framework for the simulation and the analysis of events.

The paper is organized as follows. In sect. II, a brief description of the model is presented. In sect. III, the signal

*Electronic address: yasaman@theory.ipm.ac.ir

and background events are identified and tools for establishing the simulation and analysis framework are introduced. The signal and background cross sections are then calculated. In sect. IV, the number of expected events at LHC collected with a beam of 14 TeV center of mass energy after 30 fb^{-1} integrated luminosity is calculated. Full set of kinematic cuts are designed step by step and their efficiencies on both signal and background events are calculated and shown in tables. The signal significance for each studied category and each final state is calculated. In sect. V, a brief discussion on the possibility of measuring the model parameters is presented. In sect. VI, an alternative discovery channel is presented. In sect. VII, the discovery potential of the 7 TeV run of the LHC is discussed. The paper ends with a conclusion section on the discovery potential of the model and its new particles.

II. THE MODEL

The model has a minimalistic content and adds only the following fields to the Standard Model:

- Two (or more) right-handed neutrinos, N_i ;
- A scalar SU(2) doublet Φ which carries hypercharge: $\Phi = (\phi^0 \ \phi^-)$ where $\phi^0 = (\phi_1 + i\phi_2)/\sqrt{2}$ with real ϕ_1 and ϕ_2 ;
- A singlet scalar η .

A Z_2 symmetry is imposed on the model under which these new particles are odd but the SM particles are even. The Z_2 symmetry forbids the Yukawa coupling of form $\bar{N}\Phi \cdot L$ and makes the lightest particle stable. The general Z_2 invariant renormalizable Lagrangian involving the scalars can be written as

$$\begin{aligned} \mathcal{L} = & -m_\Phi^2 \Phi^\dagger \cdot \Phi - \frac{m_s^2}{2} \eta^2 - (m_{\eta\Phi} \eta (H^T (i\sigma_2) \Phi) + \text{H.c.}) \\ & - \lambda_1 |H^T (i\sigma_2) \Phi|^2 - \text{Re}[\lambda_2 (H^T (i\sigma_2) \Phi)^2] - \lambda_3 \eta^2 H^\dagger H - \lambda_4 \Phi^\dagger \cdot \Phi H^\dagger \cdot H \\ & - \frac{\lambda'_1}{2} (\Phi^\dagger \cdot \Phi)^2 - \frac{\lambda'_2}{2} \eta^4 - \lambda'_3 \eta^2 \Phi^\dagger \cdot \Phi \\ & - m_H^2 H^\dagger \cdot H - \frac{\lambda}{2} (H^\dagger \cdot H)^2. \end{aligned} \quad (1)$$

We are interested in the regime that only the standard Higgs, H , acquires a vacuum expectation value so the Z_2 symmetry is maintained. After the electroweak symmetry breaking, the third term in Lagrangian (1) leads to a mixing between η and the neutral component of Φ . For simplicity, we take the CP invariant case so $m_{\eta\Phi}$ will be real and as a result, η will mix only with the CP-even component of ϕ^0 . The mass eigenstates δ_1 and δ_2 can be written as

$$\begin{bmatrix} \delta_1 \\ \delta_2 \end{bmatrix} = \begin{bmatrix} \cos \alpha & -\sin \alpha \\ \sin \alpha & \cos \alpha \end{bmatrix} \begin{bmatrix} \eta \\ \phi_1 \end{bmatrix} \quad (2)$$

with

$$\tan 2\alpha = \frac{2v_H m_{\eta\Phi}}{m_{\phi_1}^2 - m_\eta^2}, \quad (3)$$

$$m_{\delta_1}^2 \simeq m_\eta^2 - \frac{(m_{\eta\Phi} v_H)^2}{m_{\phi_1}^2 - m_\eta^2} \quad \text{and} \quad (4)$$

$$m_{\delta_2}^2 \simeq m_{\phi_1}^2 + \frac{(m_{\eta\Phi} v_H)^2}{m_{\phi_1}^2 - m_\eta^2} \quad (5)$$

in which

$$m_\eta^2 = m_s^2 + \lambda_3 \frac{v_H^2}{2}$$

and

$$m_{\phi_1}^2 = m_\Phi^2 + \lambda_4 \frac{v_H^2}{2} + \lambda_1 \frac{v_H^2}{2} + \lambda_2 \frac{v_H^2}{2}.$$

The CP-odd component of Φ remains mass eigenstate with mass eigenvalue

$$m_{\phi_2}^2 = m_\Phi^2 + \lambda_4 \frac{v_H^2}{2} + \lambda_1 \frac{v_H^2}{2} - \lambda_2 \frac{v_H^2}{2}.$$

The mass of the charged component of Φ is

$$m_{\phi^-}^2 = m_\Phi^2 + \lambda_4 \frac{v_H^2}{2}.$$

Terms involving right-handed neutrinos are

$$\mathcal{L} = -g_{i\alpha} \bar{N}_i \Phi^\dagger \cdot L_\alpha - \frac{M_{N_i}}{2} \bar{N}_i^c N_i, \quad (6)$$

where L_α is the lepton doublet of flavor α : $L_\alpha^T = (\nu_{L\alpha} \ell_{L\alpha}^-)$. As shown in [3], this coupling at one-loop level leads to the neutrino mass matrix as follows

$$(m_\nu)_{\alpha\beta} = \sum_i g_{i\alpha} g_{i\beta} A_i^2 \quad (7)$$

where

$$A_i^2 \equiv \frac{m_{N_i}}{32\pi} \left[\sin^2 \alpha \left(\frac{m_{\delta_2}^2}{m_{N_i}^2 - m_{\delta_2}^2} \log \frac{m_{N_i}^2}{m_{\delta_2}^2} - \frac{m_{\delta_1}^2}{m_{N_i}^2 - m_{\delta_1}^2} \log \frac{m_{N_i}^2}{m_{\delta_1}^2} \right) + \frac{m_{\phi_2}^2}{m_{N_i}^2 - m_{\phi_2}^2} \log \frac{m_{N_i}^2}{m_{\phi_2}^2} - \frac{m_{\delta_2}^2}{m_{N_i}^2 - m_{\delta_2}^2} \log \frac{m_{N_i}^2}{m_{\delta_2}^2} \right].$$

With only one right-handed neutrino, the neutrino mass matrix will have two zero mass eigenvalues and cannot accommodate the neutrino data. The model has to include at least two right-handed neutrinos. From Eq. (7), it is straightforward to show that with only two right-handed neutrinos, the determinant of the neutrino mass matrix vanishes which means one of the neutrino mass eigenvalues is zero and the neutrino mass scheme is hierarchical. By adding another right-handed neutrino non-hierarchical neutrino mass scheme can also be obtained. Here, we however concentrate on the most economic case with only two right-handed neutrinos. In the appendix, we derive constraints on the flavor structure of the couplings from the neutrino mass matrix. As shown in the appendix, in the case of inverted hierarchical scheme $|g_{i\mu}| \simeq |g_{i\tau}|$. Two specific solutions leading to normal hierarchical mass schemes for neutrinos are shown in Tab. I. To obtain these results, we have set $\Delta m_{sun}^2 = 8 \times 10^{-5} \text{ eV}^2$ and $\Delta m_{atm}^2 = 2.5 \times 10^{-3} \text{ eV}^2$ and $\lambda_2 = 0$ which leads to $m_{\phi_1} = m_{\phi_2}$. N_2 is taken to be heavy and the mixing between η and ϕ_1 is taken to be 0.01. θ is the arbitrary mixing angle that appears in the coupling structure (see Eqs. (A1,A2)). Notice that by varying m_{ϕ_1} and λ_2 (*i.e.*, parameters determining the heavy sector masses), the flavor structure (*i.e.*, $g_{i\alpha}/g_{i\beta}$) does not change. Taking $m_{\phi_1} = m_{\phi_2} = 150 \text{ GeV}$, $g_{1\alpha}$ is derived from Eq. (A1) in the appendix and shown in the last line of the table.

In this model, δ_1 , being the lightest new particle and therefore stable, plays the role of the dark matter. We shall call δ_1 ‘‘SLIM’’. Dark matter abundance is fixed by

$$\langle \sigma(\delta_1 \delta_1 \rightarrow \nu_{L\alpha} \nu_{L\beta}) v_r \rangle = \langle \sigma(\delta_1 \delta_1 \rightarrow \bar{\nu}_{L\alpha} \bar{\nu}_{L\beta}) v_r \rangle = \frac{\sin^4 \alpha}{8\pi} \left| \sum_i \frac{g_{i\alpha} g_{i\beta} m_{N_i}}{m_{\delta_1}^2 + m_{N_i}^2} \right|^2 = 3 \cdot 10^{-26} \text{ cm}^3/\text{sec}. \quad (8)$$

As shown in [3], by combining the information on σ_{tot} from the dark matter abundance with m_ν , we find

$$m_{\delta_1} < m_{N_1} \sim \text{few MeV}.$$

That is while the other scalar particles, δ_2 , ϕ_2 and ϕ^- have to be heavy enough to avoid the direct bounds from accelerators. The strongest model-independent direct bound on the charged Higgs is 80 GeV [4] and the bound on m_{δ_2} and m_{ϕ_2} is about 90 GeV [5]. At first sight, it might seem counterintuitive that while W^- and ϕ^- with $m_{\phi^-} = 80 \text{ GeV}$ have the same mass and charge, the former is already discovered but such a ϕ^- has escaped detection. This can be explained by the difference in their spin: In the process $f\bar{f} \rightarrow \gamma^* \rightarrow \phi^- \phi^+$, the angular momentum conservation implies that the final particles should be produced in the p -wave which gives rise to a suppression by an extra factor of $(1 - 4m_{\phi^-}^2/s)$ which for the maximum LEP energy amounts to 0.4. Moreover, the $W^- W^+$ production

| | Point A | Point B |
|--------------------|---|---|
| m_{N_1} (MeV) | 1 | 1 |
| m_{N_2} | $> m_{\phi^-}$ | $> m_{\phi^-}$ |
| α | 0.01 | 0.01 |
| λ_2 | 0 | 0 |
| m_{ϕ_2} (GeV) | 90 | 90 |
| θ | $\pi/2$ | 0 |
| $g_{1\alpha}$ | $\begin{pmatrix} 0 \\ 0.03 \\ 0.03 \end{pmatrix}$ | $\begin{pmatrix} 0.01 \\ 0.01 \\ -0.01 \end{pmatrix}$ |

TABLE I: Model parameters.

can take place via the t -channel neutrino exchange which has no counterpart in the $\phi^+\phi^-$ production. To our best knowledge, no analysis has been carried out on the Tevatron data that applies to our model. In principle, valence quarks and antiquarks inside the proton and antiproton beams at Tevatron can give rise to the $\phi^+\phi^-$ production via the s -channel Z^*, γ^* exchanges. However, each of the valence quarks on average carries only about 0.16 of the proton energy so the effective center of mass energy will be around 300 GeV ($\simeq 0.16 \times 2$ TeV). As a result like the LEP case, the production rate at Tevatron will be suppressed. The same process also plays the dominant role in the $\phi^+\phi^-$ production at the LHC but in the case of the LHC, the antiquark taking part in the production will be a sea quark which on average carries a lower fraction of the proton energy, $\langle x_{\bar{q}} \rangle \simeq 0.027$. The average center of mass energy of quark antiquark pair for the 14 TeV run will be $\sqrt{\langle x_q \rangle \langle x_{\bar{q}} \rangle} E_{cm} \simeq 800$ GeV which is still higher than that for the Tevatron despite the fact that in the case of the Tevatron, the quark antiquark pair are both valence quarks but in the case of the LHC one of the quarks is a sea quark. We shall discuss the effect in detail. As we shall demonstrate the discovery chance rapidly increases with center of mass energy so the discovery potential of the Tevatron cannot be significant comparing to that of the LHC. In addition to quark antiquark annihilation mode, $\phi^+\phi^-$ can be produced via gluon fusion. Similar consideration holds for the production of δ_2 and ϕ_2 . As we shall see, the suppression discussed above has the negative consequence for our analysis: The signal for the ϕ^- production suffers from large background from the W^- production.

This model has similarities with the so-called inert model [6] but here we have an extra singlet scalar and the main annihilation mode of dark matter pair is into neutrinos. Nevertheless, the contribution to the oblique parameters in our model is similar to that in the inert model. Like the inert model, the new contribution to the oblique parameters can cancel the one from a SM Higgs so heavier masses for Higgs can be made compatible with the SM. Throughout this paper, we assume that m_{ϕ^-} is equal or lighter than m_{δ_2} and m_{ϕ_2} . Moreover, we shall assume that $m_{\phi_2} - m_{\phi^-}$, $m_{\delta_2} - m_{\phi^-}$ and $|m_{\delta_2} - m_{\phi_2}|$ do not exceed 80 GeV to forbid two body decays $\delta_2, \phi_2 \rightarrow W^+\phi^-$ or $\phi_2 \rightarrow \delta_2 Z$ (or $\delta_2 \rightarrow \phi_2 Z$). This assumption is just for simplicity of the analysis. Probing the whole parameter space is beyond the scope of the present paper.

In this model, ϕ^- dominantly decays via the $g_{i\alpha}$ couplings:

$$\Gamma(\phi^- \rightarrow l_\alpha N_i) = \frac{|g_{i\alpha}|^2 (m_{\phi^-}^2 - m_{N_i}^2)^2}{16\pi m_{\phi^-}^3} \quad \text{for } m_{N_i} < m_{\phi^-}. \quad (9)$$

As discussed earlier, N_1 has to be light so decay modes $\phi^- \rightarrow N_1 e^-$, $N_1 \mu^-$ and $N_1 \tau^-$ are guaranteed to exist. If the mass of the other right-handed neutrino, N_k , is lighter than m_{ϕ^-} but $m_{N_k} \sim m_{\phi^-}$, by studying the energy spectrum of the emitted charged lepton, one can in principle distinguish between this decay and $\phi^- \rightarrow \ell_\alpha^- N_1$. Moreover, M_{N_k} and $|g_{k\alpha}|$ can in principle be derived. If for all k larger than one $m_{N_k} > m_{\phi^-}$, the decay mode $\phi^- \rightarrow N_k \ell_\alpha^-$ is not open so the decay mode ($\phi^- \rightarrow \ell_\alpha^- + \text{missing energy}$) gives only $|g_{1\alpha}|^2$. In case that $m_{N_k} \sim m_{N_1}$, it will not in practice be possible to distinguish between N_1 and N_k so the signal ($\phi^- \rightarrow \ell_\alpha^- + \text{missing energy}$) will practically yield $\sum_i |g_{i\alpha}|^2$ where the sum runs over all N_i for which $m_{N_i} < m_{\phi^-}$. In this paper, we focus on the case with only two N_i with $m_{N_2} > m_{\phi^-}$. Apart from this decay mode, ϕ^- can have other decay modes such as $\phi^- \rightarrow W^- \delta_1$, $\phi^- \rightarrow \delta_1 \ell_\alpha^- \nu$ and $\phi^- \rightarrow \delta_1 W^- \gamma$ which as seen from Fig. 1 are all subdominant for values of $g_{1\alpha} \gtrsim 0.01$ and $\sin \alpha \lesssim 0.01$.

The hypercharge of the new doublet, Φ , is the same as that of H_d in the MSSM. Thus, in the limit that $\langle H_d \rangle$ vanishes (*i.e.*, $\tan \beta \rightarrow 0$) and the η - ϕ mixing goes to zero (*i.e.*, $\alpha \rightarrow 0$), the gauge interactions of ϕ_2 and ϕ^\pm are similar respectively to those of A^0 and H^\pm . Depending on the value of m_{ϕ_1} , δ_2 will have similar gauge interactions as any of the CP-even Higgses, h or H within the MSSM. The pair production of these particles at the LHC takes

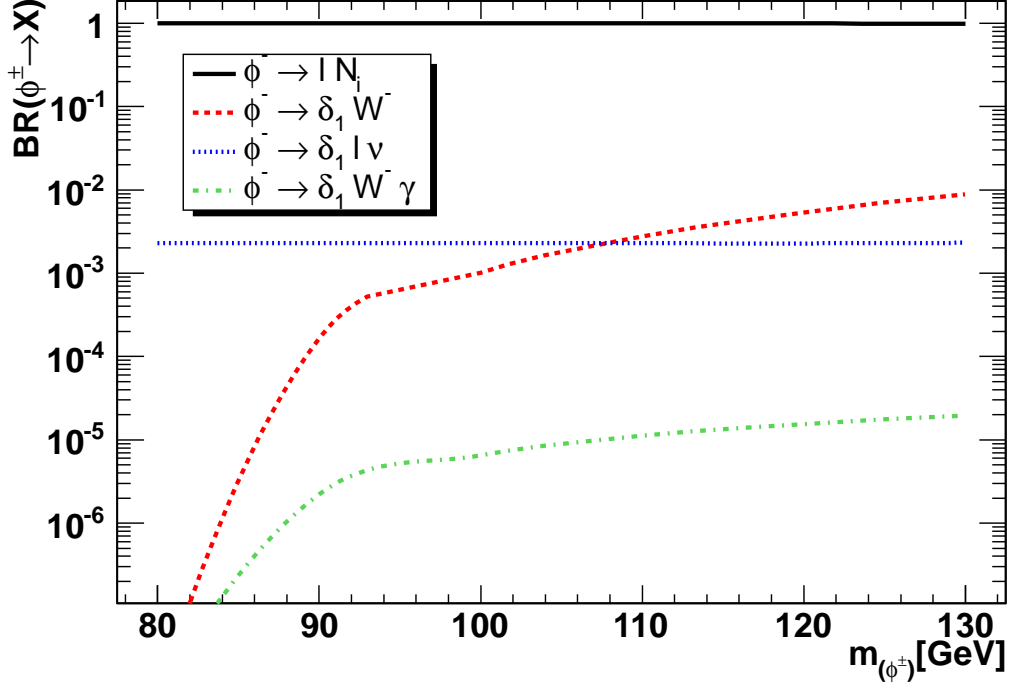


FIG. 1: Branching ratio of ϕ^\pm decays as a function of its mass. Point A from Tab. I has been used as input for this calculation.

place through the electroweak interactions. That is the $\phi^+\phi^-$, $\phi^\pm\phi_2$ and $\phi^\pm\delta_2$ production are respectively similar to H^+H^- , $H^\pm A^0$ and $H^\pm h(H)$ production within the MSSM with $\tan\beta \rightarrow \infty$. However, the Yukawa couplings of Φ in our model is quite different from those of H_d within the MSSM. As a result, the decay processes for the Φ components differ from those for the Higgs components. Neutral CP-odd Higgs within the MSSM can be singly produced via gluon fusion but the parallel does not exist within this model in which Yukawa coupling between Φ and the b quarks are forbidden.

To perform our analysis, we focus on the points shown in Tab. I. The point A in Table I is chosen to search for tauonic and muonic final states while the point B is used to search for final states involving electrons. The point A in the parameter space leads to a negligible branching ratio for ϕ^- decay to electrons while decay to a μ or τ lepton is possible with equal probability. That is at point A, $\text{BR}(\phi^\pm \rightarrow \mu^\pm N_1) = \text{BR}(\phi^\pm \rightarrow \tau^\pm N_1) \simeq 0.5$. Figure 1 shows the contributions from all the decay channels and verifies that the above approximation is valid up to a maximum 1% error for $m_{(\phi^\pm)} = 130$ GeV.

In this scenario three samples of events are expected corresponding to different final states: $\mu\mu$, $\mu\tau$ and $\tau\tau$. The $\tau\tau$ final state suffers from the large hadronic backgrounds such as W +jets with W decaying to τ or jets. These background events may survive due to light jets faking the τ .

As we shall see, the $\mu\mu$ and $\mu\tau$ final states can be observed with a significance exceeding 5σ at $30fb^{-1}$. The next sections are devoted to signal and background simulation. The event analysis and selection is then described based on the kinematic cuts applied in order to increase the signal to background ratio. A full study of kinematic distributions is performed and a dedicated τ jet identification is applied similar to the standard LHC algorithms in Ref. [7]. Finally the signal significance is estimated for each search category and final state.

III. SIGNAL AND BACKGROUND SIMULATION

Considering the above observation the ϕ^\pm pair production is generated using the process $pp \rightarrow H^+H^-$ setting $\tan\beta = 100$ which is reasonably high. These events are generated using PYTHIA 8.1.2.5 [8]. To account for the τ leptons proper decays, TAUOLA package [9] is used. Since PYTHIA 8 is based on C++ programming language, TAUOLA C++ interface [10] is used to link TAUOLA and PYTHIA 8 for the correct production of τ hadronic decays. Since TAUOLA interface output is in the HepMC format, HepMC 2.5.1 [11] is linked to TAUOLA interface and is

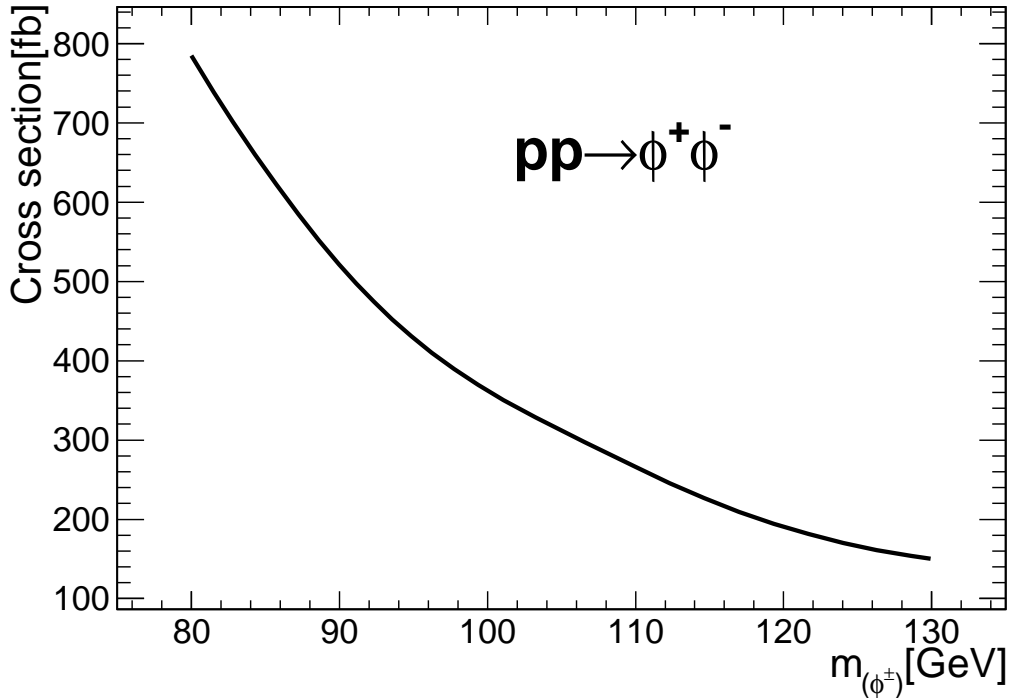


FIG. 2: Signal cross section as a function of m_{ϕ^\pm} .

| Process | W^+W^- | $t\bar{t}$ | W+jets | Z+jets |
|---------------|--------------------|--------------------|--------------------|--------------------|
| Cross Section | 115.5 ± 0.4 pb | 878.7 ± 0.5 pb | 187.1 ± 0.1 nb | 258.9 ± 0.7 nb |

TABLE II: Background cross sections calculated using MCFM package.

used in the analysis.

Throughout the analysis, the τ leptons are identified through their hadronic decays which results in a narrow τ jet which will be described in detail later in the next sections.

The jet reconstruction is performed using FASTJET 2.4.1 [12] with anti-kt algorithm [13] and a cone size of 0.4 and the E_T recombination scheme.

The signal cross section is calculated using PYTHIA. As mentioned earlier, the charged Higgs pair production is expected to simulate ϕ^\pm events if a large enough $\tan\beta$ is used. Since the signal cross section decreases rapidly with increasing m_{ϕ^\pm} , the low mass ϕ^\pm is studied in this analysis. Figure 2 shows the signal cross section as a function of m_{ϕ^\pm} . The main background events are W^+W^- , $t\bar{t}$, W+jets and Z+jets. Their cross sections are calculated using MCFM 5.7 [14] at NLO. Table II shows the background cross sections calculated using MCFM with renormalization and factorization scale set to the top quark mass (172.5 GeV) for $t\bar{t}$ events, the W boson mass (80.4 GeV) for W^+W^- and W+jets events and the Z boson mass (91 GeV) for Z+jets events. For both event simulation and cross section calculation purposes, MRST 2004 NNLO PDF is used by linking LHAPDF 5.8.1 [15] to the PYTHIA event generator as well as MCFM.

In order to calculate the expected number of events at $30fb^{-1}$, the total cross sections in Table II are multiplied by the proper branching ratios. For $t\bar{t}$ events, while one of W bosons (from t or \bar{t} decay) decays to a muon, the other W, is forced to decay to a τ lepton or light jets. The same decay channel is considered for W^+W^- events. The W boson decay to light jets is considered to account for the τ jet fake rate from light jets. For W+jet events, the W boson is forced to decay to a muon and appearance of a τ jet is only possible again through the τ jet fake rate. The Z+jets process is only considered for the $\mu\mu$ final state and the Z boson is forced to decay to a pair of muons. In this analysis the following values are used for branching ratio of W and Z bosons according to Particle Data Group [16]: $BR(W^+ \rightarrow \mu^+\nu) = 10.57\%$, $BR(W^+ \rightarrow \tau^+\nu) = 11.25\%$, $BR(W^+ \rightarrow \text{hadrons}) = 67.60\%$, $BR(Z \rightarrow \mu\mu) = 3.36\%$.

As is seen from Table II, a large suppression factor is needed due to the large background cross sections. In the

next sections, it is shown that a reasonable background suppression can be achieved by applying kinematic cuts and using a state-of-the-art τ identification and selection.

IV. EVENT KINEMATICS

As mentioned earlier in this analysis only two final states of $\mu\mu$ and $\tau\mu$ from $\phi^+\phi^-$ decay are considered. In the following, two separate analyses are designed and described in detail. It is convenient to define the transverse energy, E_T , as

$$E_T \equiv \sqrt{p_x^2 + p_y^2}$$

where the z direction is taken parallel to the beam direction.

A. The $\tau\mu E_T^{miss}$ Final State

This final state is searched for by requiring one muon and one τ jet. The muon transverse momentum distribution has been shown in Fig. 3. The small contribution from soft muons in τ lepton decays (see Fig. 4), can be viewed as a small excess in signal and background events. In the signal events, in the search for $\tau\mu E_T^{miss}$ final state, this contribution may come from $pp \rightarrow \phi^+\phi^- \rightarrow \tau\tau E_T^{miss}$, with one τ decaying hadronically and the other decaying to a muon. However, due to the small branching ratio of τ decay to muons ($\sim 17\%$) and the soft p_T distribution of these muons, no sizable contribution from these events is expected. The same considerations hold for muonic decays of the τ leptons in background events like $t\bar{t}$ and WW . As a result, the τ leptons mainly contribute in the analysis through their hadronic decays. The following kinematic requirement is applied on muons in the event:

$$p_T^\mu > 50 \text{ GeV}, \quad |\eta| < 2.5. \quad (10)$$

where η is the pseudorapidity defined as

$$\eta \equiv -\log \left[\tan \frac{\theta}{2} \right]$$

in which θ is the angle between the momentum and the beam axis. This kinematic cut is applied mainly to suppress backgrounds with soft muons in the final state such as W +jets.

The τ jet identification is performed by first reconstructing jets and requiring kinematic cuts as the following:

$$E_T^{\text{jet}} > 30 \text{ GeV}, \quad |\eta| < 2.5. \quad (11)$$

A reconstructed jet which passes the above requirement is considered as a τ jet candidate. All selected jets should be separated enough from muons with $p_T > 20 \text{ GeV}$ with the following requirement:

$$\Delta R_{(\text{jet}, \mu)} > 0.4. \quad (12)$$

Here ΔR is defined as $\Delta R = \sqrt{(\Delta\eta)^2 + (\Delta\phi)^2}$ where η is the pseudorapidity and ϕ is the azimuthal angle with respect to the collider beam axis. Figure 5 shows the transverse energy distribution of selected jets and the number of reconstructed jets passing above requirements are shown in Figure 6. Due to the requirements of Eq. 11 and 12, some signal events are killed, however, a larger fraction of background events fall in zero jet bin. The single W production has the largest cross section when produced with no jet so a large fraction of them fill the zero jet bin. Another reason is the fact that the jet accompanying the W boson is usually a spectator quark flying in the forward-backward direction and as a result, failing the requirement of Eq. 11. The τ hadronic decay produces predominantly one or three charged pions with a sizably high transverse momentum due to the low charged track multiplicity compared to the light quark jets. The leading track associated to the jet is found by searching for the highest- p_T track in the matching cone defined around the jet axis with an opening angle of $\Delta R < 0.1$.

The desired polarization of the τ leptons in ϕ^\pm decays is not simulated by using charged Higgs events in PYTHIA because of opposite polarizations between the PYTHIA charged Higgs events and our model. Thus, in this analysis polarization dependent cuts on leading track p_T , the ratio of leading track p_T over τ jet energy, and E_T^{miss} are removed. The TAUOLA package is still needed to get correct branching ratio of τ lepton decays and produce hadronic decays

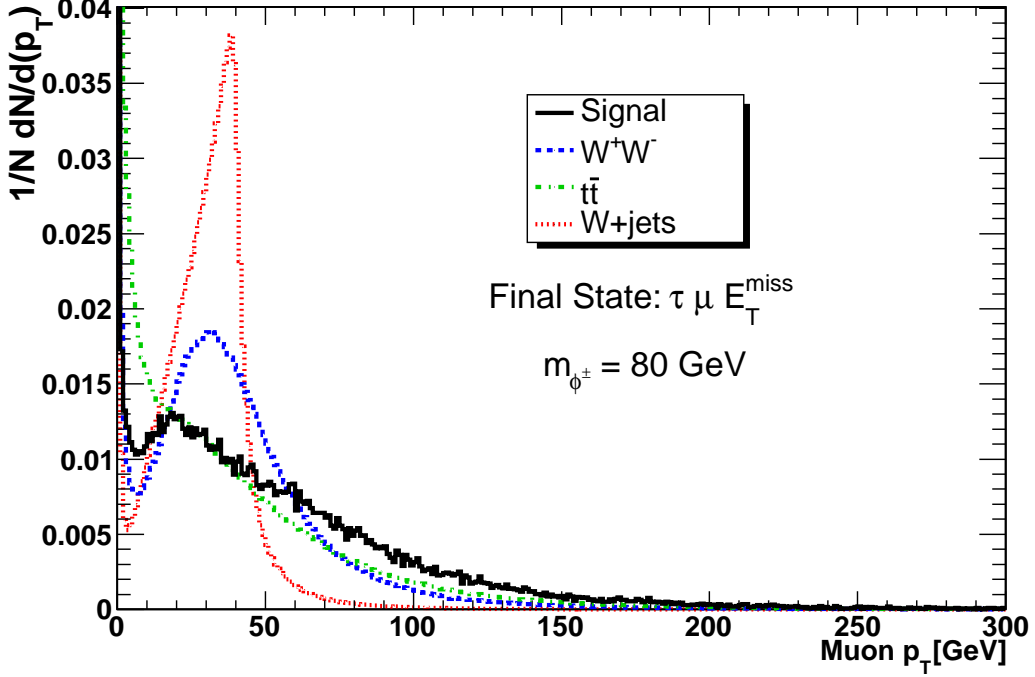


FIG. 3: Muon transverse momentum distributions in signal and background events in the $\tau\mu E_T^{miss}$ final state.

with proper charged track multiplicity and decay topology. The rest of τ identification algorithm is applied as the following. The isolation cone is defined with a cone size of $\Delta R < 0.4$ around the leading track. The signal cone is also defined around the leading track with $\Delta R < 0.07$. The isolation is applied by requiring no charged track with $p_T > 1$ GeV to be in the isolation annulus defined as $0.07 < \Delta R < 0.4$. This requirement suppresses light quark jets which contain many charged tracks in their isolation annulus.

To further suppress the fake τ jet rate and increase the τ jet purity in events with genuine τ jets, a search for charged tracks in the signal cone is made and the number of tracks in the signal cone is required to satisfy the following requirement:

$$\text{Number of signal tracks} = 1 \text{ or } 3. \quad (13)$$

Figure 7 shows distribution of the number of signal tracks in signal events before applying the cut. As seen from Fig. 7, τ jets have undergone 1- or 3-prong decays predominantly. The muons and τ leptons are expected to be produced back-to-back in the signal events. Figure 8 shows the distribution of the azimuthal angle between the two leptons. In the case of the τ leptons, the τ jet direction is used. As is observed from Fig. 8, background events also show similar distributions. Thus, no cut on $\Delta\phi$ between the muon and the τ jet is applied. In the next step, the τ lepton charge is calculated as the sum of charges of tracks in the signal cone. Since muons and τ leptons in signal events are produced with opposite charges, the following requirement is applied:

$$\text{Muon charge} + \tau \text{ jet charge} = 0. \quad (14)$$

The analysis is therefore only sensitive to the sum of charges of the two leptons and does not care whether μ and τ are individually positive or negative.

An event is selected if it passes all the above selection requirements. Table III shows selection efficiencies for signal events with $m_{(\phi^\pm)}$ ranging from 80 GeV to 130 GeV. The quoted efficiencies show fraction of events which pass a cut and contain exactly the same number of physical objects as the cut requires, *e.g.*, the fourth row shows the fraction of events having exactly one muon passing the kinematic cuts in Eq. (10).

In this analysis, selection cuts are mass independent. As is seen, the total selection efficiency increases due to harder kinematic distributions with increasing $m_{(\phi^\pm)}$. This effect is, however, compensated by decreasing cross section of signal events. Table IV shows selection efficiencies for background samples.

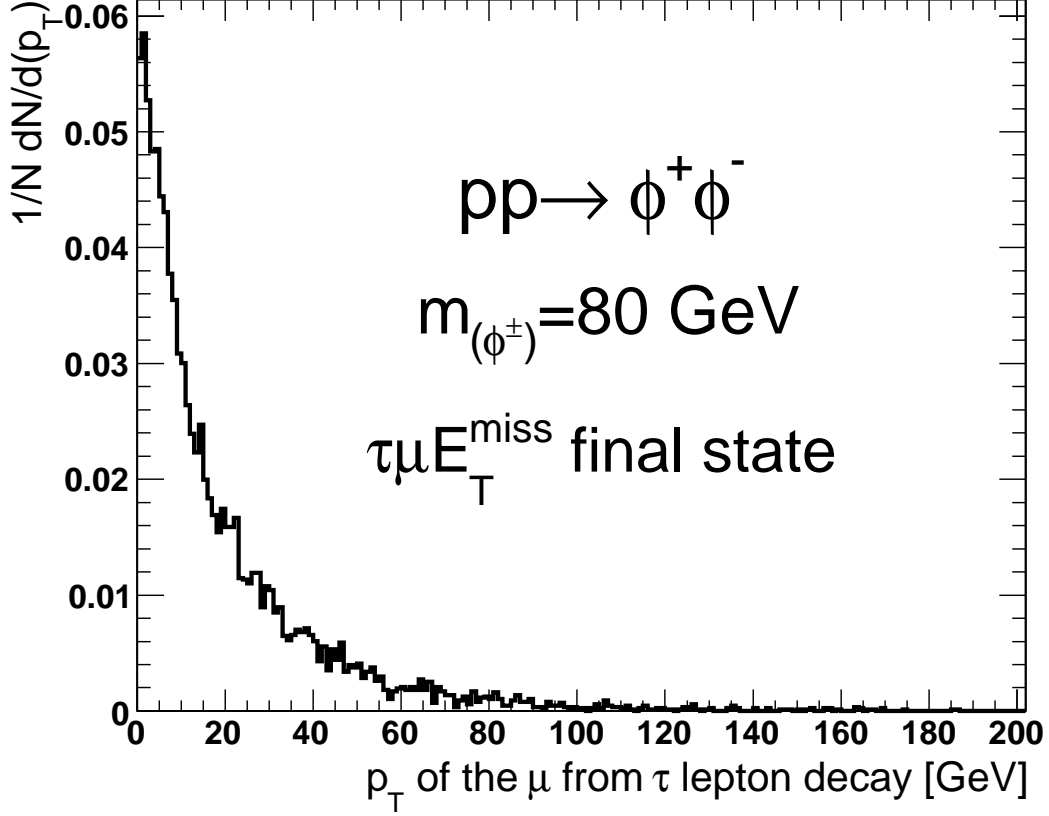


FIG. 4: Transverse momentum distribution of the muon from τ lepton decay in signal events in the $\tau\mu E_T^{miss}$ final state.

Having obtained the number of signal and background events after all selection cuts, the signal significance is now calculated as

$$\text{Signal Significance} = \frac{N_S}{\sqrt{N_B}} \quad (15)$$

where N_S (N_B) is the final number of signal (total background) events after all selection cuts. Table V shows the signal significance for different $m_{(\phi^\pm)}$ values at 30 fb^{-1} .

B. The $\mu\mu E_T^{miss}$ Final State

To search for this final state, the τ jet identification is removed from the analysis. Instead, the focus is on muon identification and E_T^{miss} distributions. Figure 9 shows the transverse momentum distributions of the muons. The muons in the events are required to satisfy the following requirements:

$$p_T^\mu > 50 \text{ GeV}, \quad |\eta| < 2.5. \quad (16)$$

An event is required to have exactly two muons passing the above requirements. As seen from Fig. 9, the soft muons in the Z +jets events which are due to the off-shell production of Z^0 bosons are removed by the above requirement and do not contribute to the signal selection. To study the number of jets in signal and background events, a jet reconstruction is performed. Figure 10 shows the number of reconstructed jets which pass the following requirements:

$$E_T^{\text{jet}} > 30 \text{ GeV}, \quad |\eta| < 2.5. \quad (17)$$

A jet is required to be separated enough from muons with $p_T > 30 \text{ GeV}$ in the event with the following requirement:

$$\Delta R_{(\text{jet}, \mu)} > 0.4. \quad (18)$$

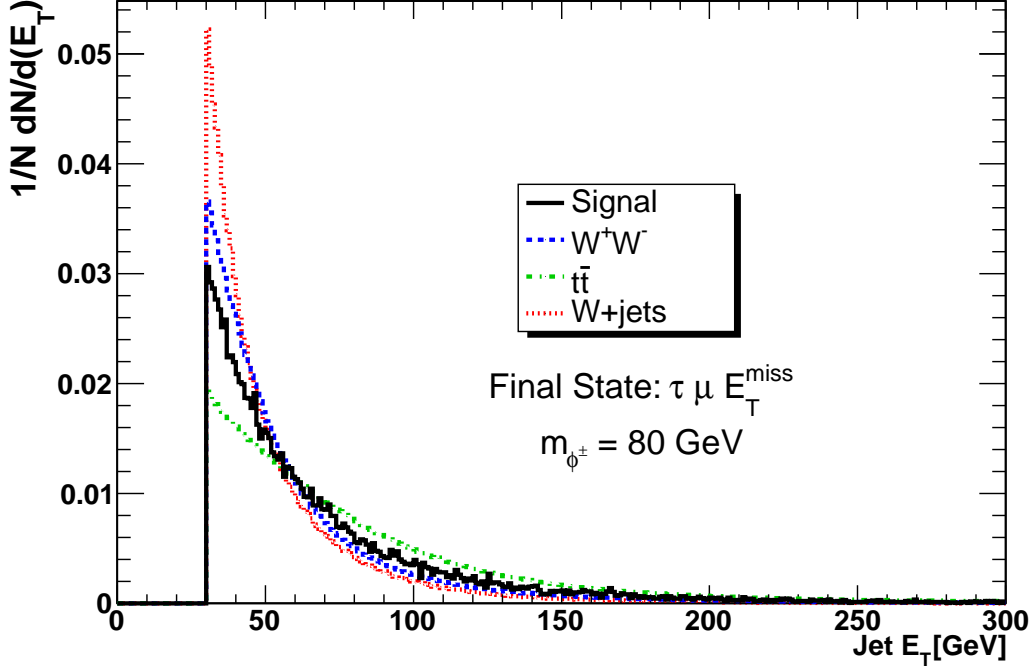


FIG. 5: Transverse energy distribution of reconstructed jets in signal and background events in the $\tau\mu E_T^{miss}$ final state. All jets satisfying Eqs. 11 and 12 fill the histogram. Softer jets with $E_T < 30$ GeV are discarded as the jet multiplicity strongly depends on the jet transverse energy and rapidly increases when soft jets are included, leading to long analysis time per event.

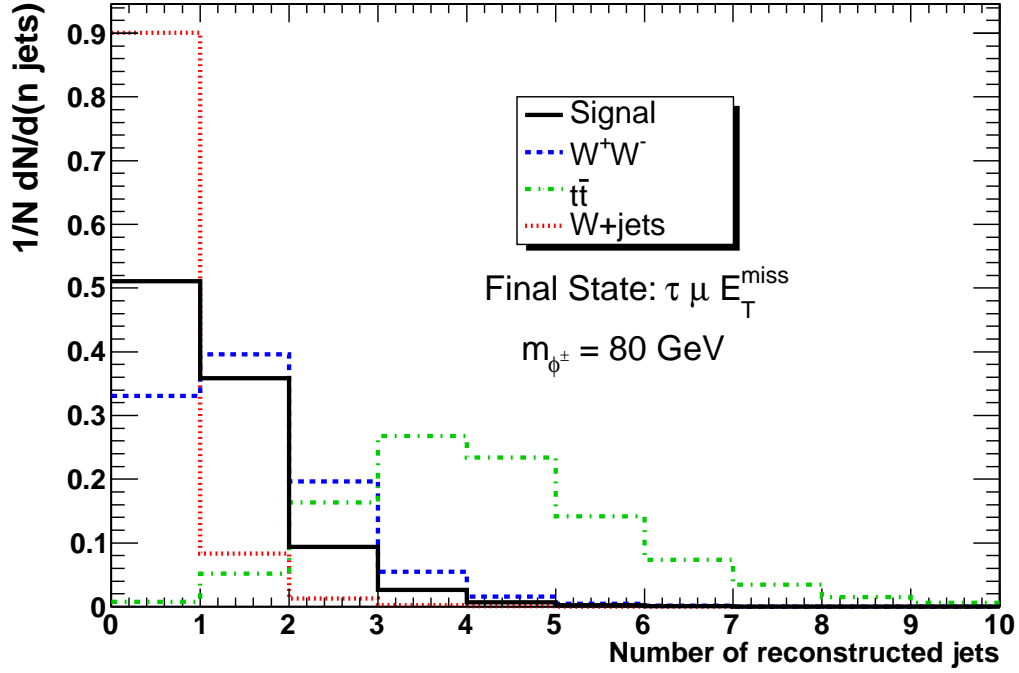


FIG. 6: Number of reconstructed jets in signal and background events in the $\tau\mu E_T^{miss}$ final state. A jet is considered and counted if it satisfies Eqs. 11 and 12.

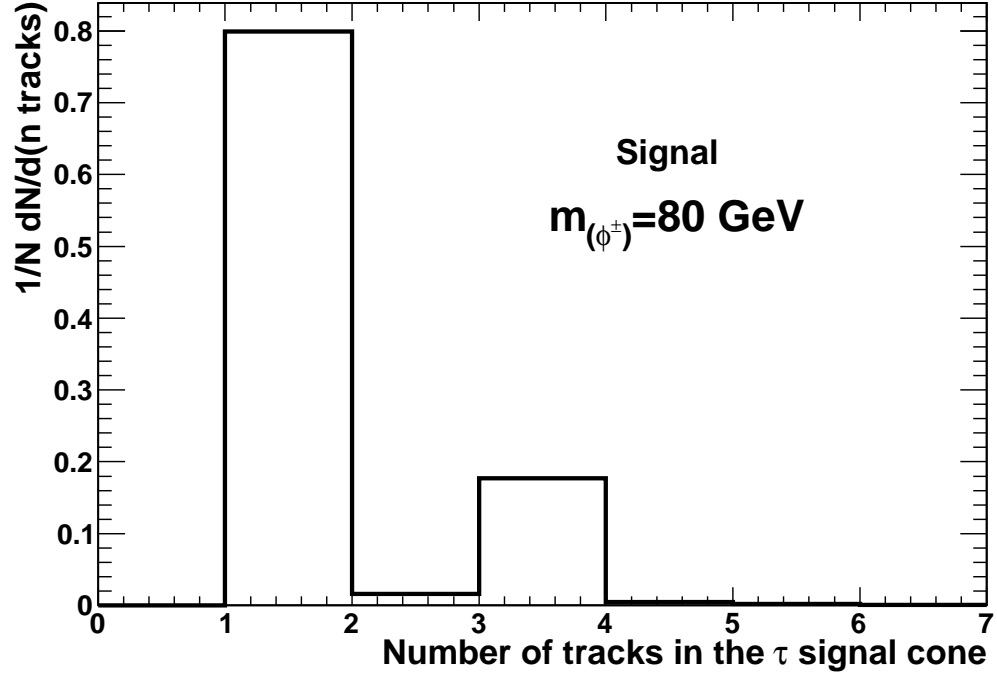


FIG. 7: Number of tracks in the signal cone around the leading track of the τ jet.

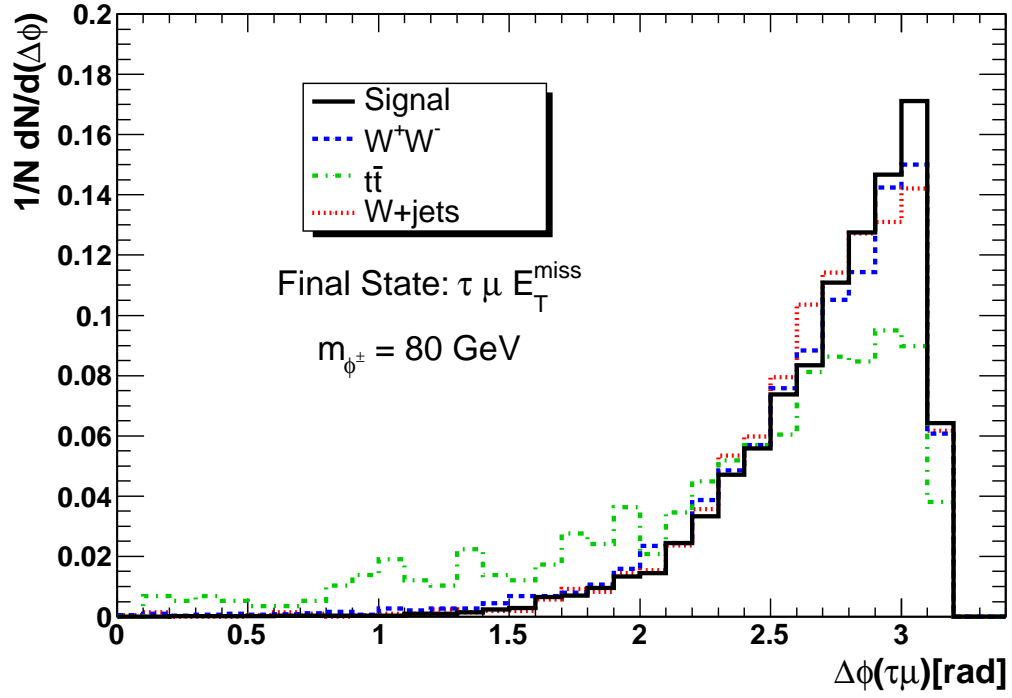


FIG. 8: The distribution of the azimuthal angle between the muon and the τ jet candidate.

| $m_{(\phi^\pm)}$ | 80 GeV | 90 GeV | 110 GeV | 130 GeV |
|---|-------------|-------------|-------------|------------|
| Total cross section [fb] | 783 | 521 | 265 | 150 |
| Number of events at 30 fb^{-1} | 11745 | 7815 | 3975 | 2250 |
| N Muons = 1 | 5018(42.7%) | 3810(48.7%) | 2251(56.6%) | 1419(63%) |
| N Jets = 1 | 2029(40.4%) | 1585(41.6%) | 976(43.4%) | 647(45.6%) |
| Isolation | 1375(67.7%) | 1101(69.4%) | 686(70.2%) | 468(72.4%) |
| 1- or 3-prong decay | 1306(95%) | 1045(94.9%) | 653(95.3%) | 447(95.5%) |
| opposite charge | 1304(99.8%) | 1043(99.8%) | 653(99.9%) | 447(99.9%) |
| total efficiency | 11.1% | 13.3% | 16.4% | 19.8% |
| Expected events at 30 fb^{-1} | 1304 | 1043 | 653 | 447 |

TABLE III: Selection efficiencies and remaining number of signal events after each cut in the $\tau\mu E_T^{miss}$ final state. Numbers in parentheses are relative efficiencies in percent with respect to the previous cut. Branching ratios have been taken into account in transition from the second to third row, thus the number of events at 30 fb^{-1} has been calculated as $N = \sigma_{tot.} \times BR \times Lumi.$, where $\sigma_{tot.}$ is the value quoted in the second row, BR is the product of all branching ratios of decays taking into account the permutation factors, e.g. in this analysis it is $2 \times BR(\phi^+ \rightarrow \tau E_T^{miss}) \times BR(\phi^- \rightarrow \mu E_T^{miss})$, and $Lumi.$ is the integrated luminosity which is 30 fb^{-1} in this analysis.

| Process | W^+W^- | $t\bar{t}$ | W+jets |
|---|---------------|---------------------------|---------------------------|
| Total cross section [pb] | 115.5 | 878.7 | 187.1×10^3 |
| Number of events at 30 fb^{-1} | 577577 | 4394086 | 5.9×10^8 |
| N Muons = 1 | 142084(24.6%) | 1.8×10^6 (40.9%) | 2.5×10^7 (4.2%) |
| N Jets = 1 | 60812(42.8%) | 81512(4.5%) | 1.1×10^7 (44.5%) |
| Isolation | 8483(13.9%) | 5533(6.8%) | 953682(8.6%) |
| 1- or 3-prong decay | 4807(56.7%) | 2545(46%) | 244810(25.7%) |
| Opposite charge | 4618(96.1%) | 2241(88.1%) | 209655(85.6%) |
| total efficiency | 0.8% | 0.05% | 0.03% |
| Expected events at 30 fb^{-1} | 4618 | 2241 | 209655 |

TABLE IV: Selection efficiencies and remaining number of background events after each cut in the $\tau\mu E_T^{miss}$ final state. Numbers in parentheses are relative efficiencies in percent with respect to the previous cut. Branching ratios have been taken into account in transition from the second to third row.

Thus, to suppress the background events with jets in the final state, it is required that no jet satisfying the above requirement exists in the event. Since Z +jets events could be a potential background for $\mu\mu$ final state, the invariant mass of the two muons are plotted as shown in Fig. 11 and a cut on that is applied as the following:

$$\text{Inv. Mass}(\mu_1, \mu_2) > 120\text{ GeV} . \quad (19)$$

In the next step the azimuthal angle between two muons is plotted as shown in Fig. 12. In this analysis, we do not also apply any cut on $\Delta\phi_{(\mu_1, \mu_2)}$. As seen from Fig. 12, the Z +jets events tend to show stronger back-to-back muon pairs. This effect can be due to the fact that muons in the Z +jets events come from a single mother particle. Further suppression of this background is possible by applying a cut on this distribution e.g. $\Delta\phi_{(\mu_1, \mu_2)} < 3$. However, since the final signal significance exceeds 5σ , a study of the power of this cut and further optimization of this search is left for a full analysis including detector effects. Since the signal events are produced with opposite charges of muons, the opposite charge requirement is also applied to search for this final state:

$$\text{charge}_{(\mu_1)} + \text{charge}_{(\mu_2)} = 0 . \quad (20)$$

| $m_{(\phi^\pm)}$ | 80 GeV | 90 GeV | 110 GeV | 130 GeV |
|---------------------|--------|--------|---------|---------|
| Signal significance | 2.8 | 2.2 | 1.4 | 1 |

TABLE V: Signal significance in the $\tau\mu E_T^{miss}$ final state for different $m_{(\phi^\pm)}$ hypotheses at 30 fb^{-1} .

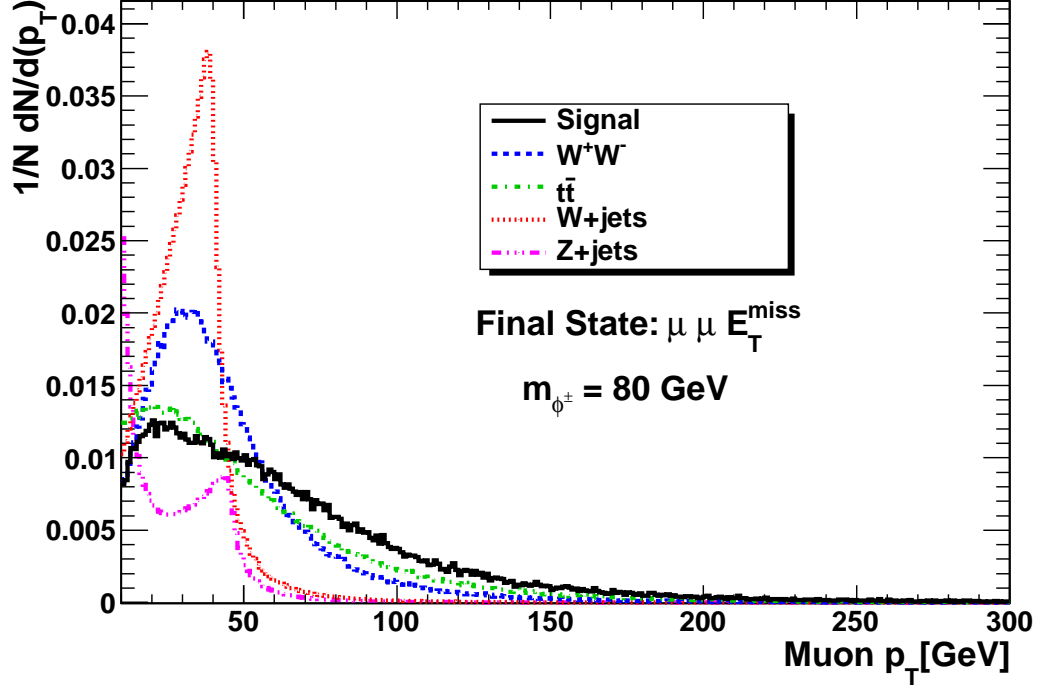


FIG. 9: Muon transverse momentum distributions in signal and background events in the $\mu\mu E_T^{\text{miss}}$ final state. This is an inclusive histogram i.e. any muon in the event satisfying kinematic cuts as in Eq. 16 has filled the histogram. Histogram starts from 10 GeV on the X-axis to suppress the large peak of soft muons from off-shell Z +jets events.

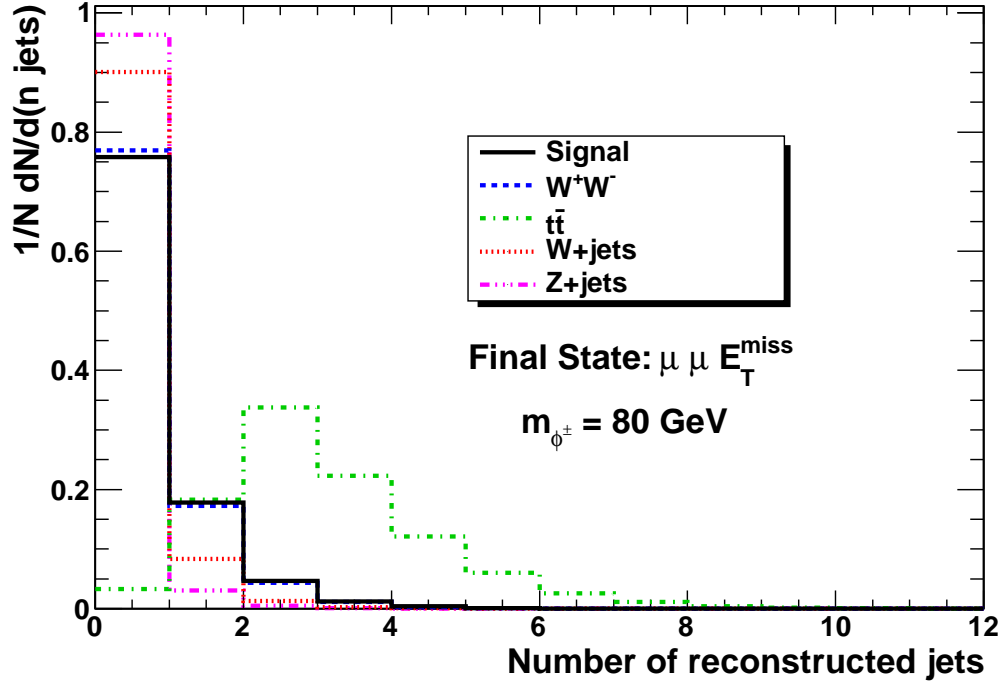


FIG. 10: Number of reconstructed jets in signal and background events in the $\mu\mu E_T^{\text{miss}}$ final state. A jet is considered and counted if it passes kinematic requirements described in the text.

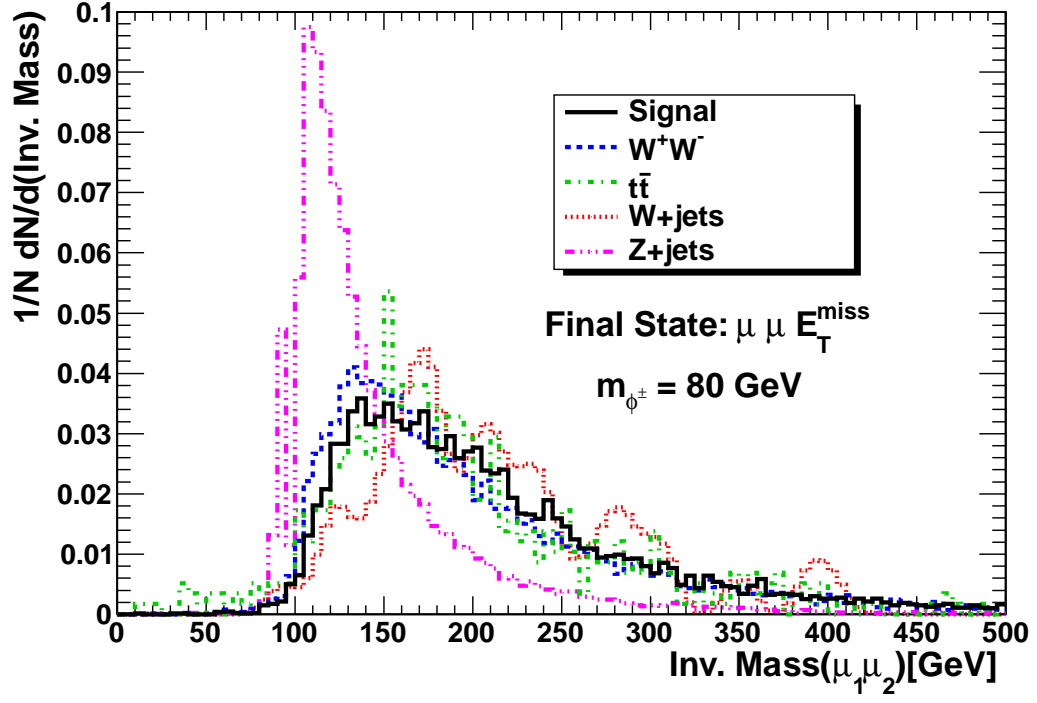


FIG. 11: Distribution of the invariant mass of the di-muon system in the $\mu\mu E_T^{\text{miss}}$ final state.

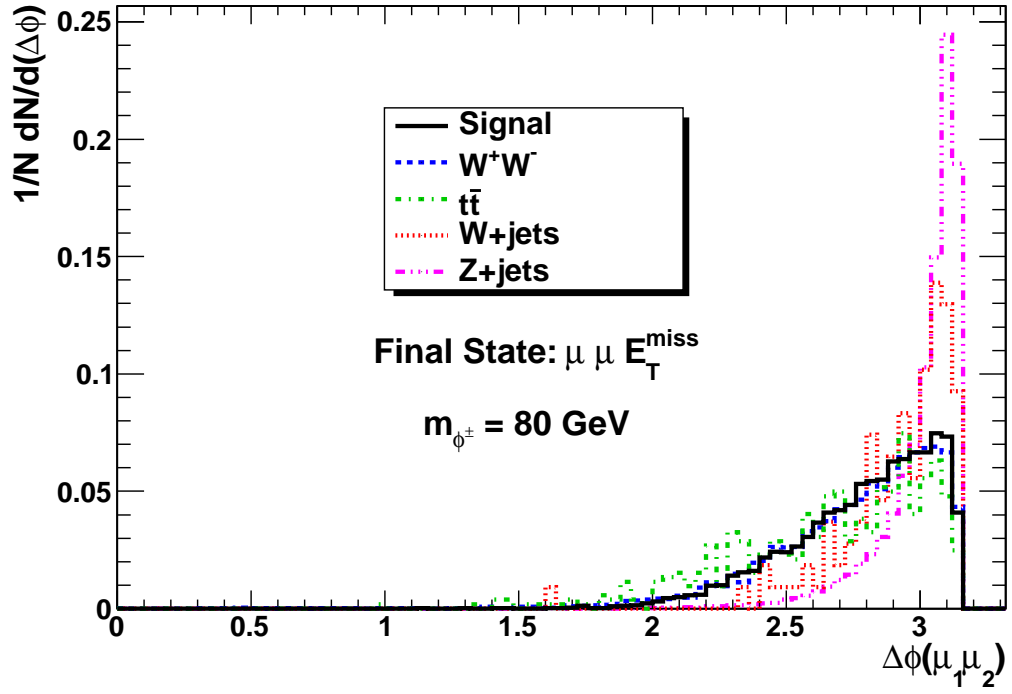


FIG. 12: The distribution of the azimuthal angle between the two muons.

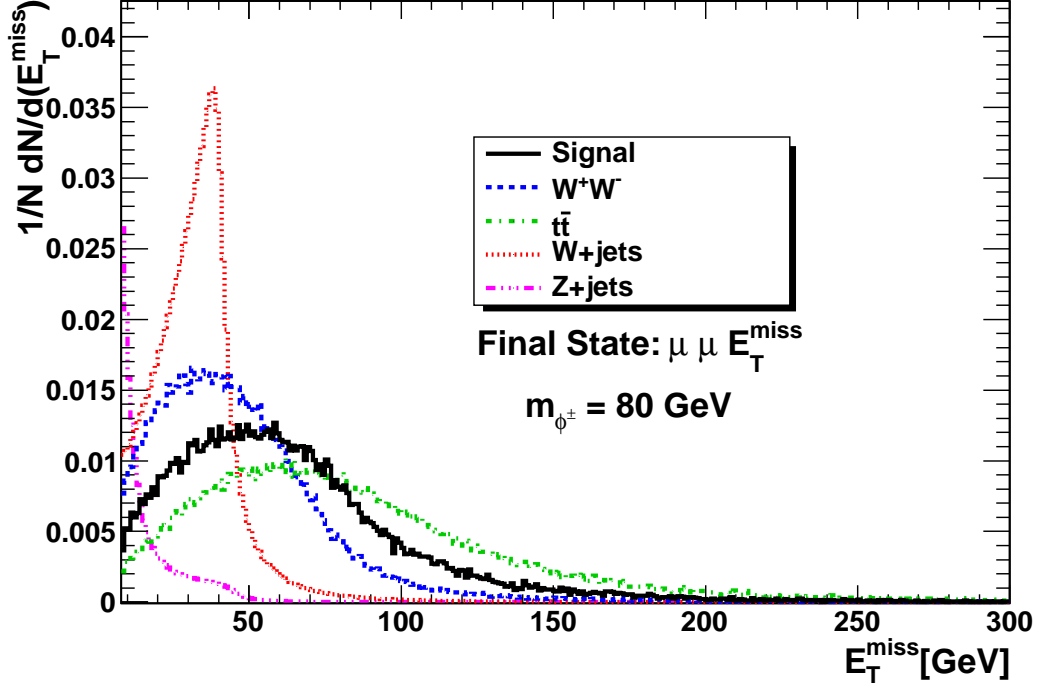


FIG. 13: Missing transverse energy distribution in the signal and background events in the $\mu\mu E_T^{\text{miss}}$ final state.

Finally the E_T^{miss} distribution is obtained using Eq. (21).

$$E_T^{\text{miss}} = \left| \sum_i \vec{p}_{T_i} \right|. \quad (21)$$

The index i runs over all stable particles in the event within the volume defined by $|\eta| < 3.5$. This volume covers barrel and endcap calorimeters. The resulting distributions are shown in Fig. 13 and a cut on E_T^{miss} is applied as the following:

$$E_T^{\text{miss}} > 50 \text{ GeV}. \quad (22)$$

Table VI shows the selection efficiencies and the remaining number of signal events after applying each cut for different $m_{(\phi^\pm)}$ hypotheses.

As can be seen the total selection efficiency increases with increasing $m_{(\phi^\pm)}$. Table VII shows selection efficiencies for background samples. In this final state, W +jets background is more suppressed due to requiring two muons in the event. While one of the muons can be genuine from the W decay, the other has to come from heavy meson decays appearing as a muon inside a jet cone. These muons are expected to be better suppressed with more sophisticated reconstruction and isolation algorithms used in the LHC full simulation analyses. The Z +jets background is also expected to be under control with the cut on E_T^{miss} and also the hard muon pair requirement. As can be seen from Fig. 9, the majority of these events tend to have either very soft muons or muons located around $E_T \simeq 45$ GeV (making the Z boson invariant mass peak). Thus, only a negligible fraction of these events appear with both muons harder than $E_T = 50$ GeV. With the number of signal and background events as obtained in Tabs. VI and VII, the signal significance is calculated as shown in Table VIII. As a rule of thumb, one can estimate the signal significance in the $ee E_T^{\text{miss}}$ final state. For this search, the point B in Table I can be used. According to the values of $g_{1\alpha}$ which are equal for $\alpha = e, \mu$ and τ , the branching ratios of the ϕ^\pm decays to different leptonic final states would be equal, *i.e.*, $BR(\phi^\pm \rightarrow e^\pm N_1) = BR(\phi^\pm \rightarrow \mu^\pm N_1) = BR(\phi^\pm \rightarrow \tau^\pm N_1) \simeq 1/3$. Since the background samples have the same cross section times branching ratios for both final states, one can use the signal significance in $\mu\mu E_T^{\text{miss}}$ and scale the numerator of Eq. 15 by a factor of $4/9$ which leads to a significance of 4.1σ for $ee E_T^{\text{miss}}$ final state for $m_{(\phi^\pm)} = 80$ GeV at 30 fb^{-1} . This estimation is based on the assumption that the kinematics of events in $\mu\mu E_T^{\text{miss}}$ and $ee E_T^{\text{miss}}$ final states are very similar. From another point of view this is a simplistic estimation as there is a difference between

| $m_{(\phi^\pm)}$ | 80 GeV | 90 GeV | 110 GeV | 130 GeV |
|---|-----------|-----------|-----------|-----------|
| Total cross section [fb] | 783 | 521 | 265 | 150 |
| Number of events at 30 fb^{-1} | 5872 | 3907 | 1987 | 1125 |
| N Muons = 2 | 1348(23%) | 1080(28%) | 720(36%) | 494(44%) |
| N Jets = 0 | 961(71%) | 763(71%) | 494(69%) | 331(67%) |
| Inv Mass(μ, μ)>120 GeV | 895(93%) | 711(93%) | 463(94%) | 308(93%) |
| Opposite charge | 895(100%) | 711(100%) | 463(100%) | 308(100%) |
| E_T^{miss} | 431(48%) | 393(55%) | 310(67%) | 231(75%) |
| total efficiency | 7.3% | 10.1% | 15.6% | 20.6% |
| Expected events at 30 fb^{-1} | 431 | 393 | 310 | 231 |

TABLE VI: Selection efficiencies and remaining number of signal events after each cut in the $\mu\mu E_T^{miss}$ final state. Numbers in parenthesis are relative efficiencies in percent with respect to the previous cut. Branching ratios have been taken into account in transition from the second to third row.

| Process | W^+W^- | $t\bar{t}$ | W+jets | Z+jets |
|---|------------|-------------------|-----------------------------|----------------------|
| Total cross section [pb] | 115.5 | 878.7 | 187.1×10^3 | 258.9×10^3 |
| Number of events at 30 fb^{-1} | 38713 | 2.9×10^5 | 5.9×10^8 | 2.6×10^8 |
| N Muons = 2 | 4120(11%) | 52867(18%) | 2635(4×10^{-4} %) | 752180(0.3%) |
| N Jets = 0 | 2925(71%) | 1705(3%) | 1219(46%) | 370599(49%) |
| Inv Mass(μ, μ)>120 GeV | 2620(90%) | 1514(89%) | 1160(95%) | 220655(59%) |
| Opposite charge | 2619(100%) | 1447(96%) | 1082(93%) | 220544(100%) |
| E_T^{miss} | 730(28%) | 937(65%) | 295(27%) | 234(0.1%) |
| total efficiency | 1.9% | 0.3% | 5×10^{-5} % | 9×10^{-5} % |
| Expected events at 30 fb^{-1} | 730 | 937 | 295 | 234 |

TABLE VII: Selection efficiencies and remaining number of background events after each cut in the $\mu\mu E_T^{miss}$ final state. Numbers in parentheses are relative efficiencies in percent with respect to the previous cut. Branching ratios have been taken into account in transition from the second to third row.

muon and electron reconstruction and selection efficiencies in the detector. There can be also some under-estimation due to the fact that in the W+jets events, the electron fake rate is higher than the muon fake rate. A detailed study of these features is beyond the scope of this paper and needs a full simulation of the detector.

V. MEASURING THE MODEL PARAMETERS

In this section, an approach for measuring model parameters is introduced and verified for the specific search described in this paper.

Having observed $N_{obs.}$ at 30 fb^{-1} , the expected number of signal events has to be extracted from the observed number of events by subtracting the contamination of the background and then dividing by the total selection efficiency of the signal events which is obtained from the simulation. In other words,

$$N_S = \frac{N_{obs.} - N_B}{\epsilon_S} \quad (23)$$

| $m_{(\phi^\pm)}$ | 80 GeV | 90 GeV | 110 GeV | 130 GeV |
|---------------------|--------|--------|---------|---------|
| Signal significance | 9.2 | 8.4 | 6.6 | 4.9 |

TABLE VIII: Signal significance in $\mu\mu E_T^{miss}$ final state for different $m_{(\phi^\pm)}$ hypotheses.

| Channel | WW | W+jets | Z+jets | $t\bar{t}$ |
|-----------------------|--------------|--------------|--------------|---------------|
| Central Cross Section | 115.5 pb | 187.1 nb | 258.9 nb | 878.6 pb |
| Ren. Scale $\times 2$ | 111.5(-3.5%) | 191.7(2.1%) | 263.1(1.6%) | 777.2(-11.5%) |
| Ren. Scale $\div 2$ | 117.7(1.9%) | 181.8(-2.8%) | 252.2(-2.6%) | 977.3(11.2%) |
| NNPDF2.0 | 114.5(-0.9%) | 185.9(-0.6%) | 285.5(10.3%) | 917.6(4.4%) |
| MSTW2008nnlo | 119.5(3.5%) | 198.1(5.9%) | 270.9(4.6%) | 861.9(-1.9%) |
| CTEQ6.6 | 113.3(-1.9%) | 196.3(4.9%) | 302.9(17%) | 841.7(-4.2%) |
| $\alpha_S=0.1127$ | 114.3(-1%) | 186.2(-0.5%) | 262.2(1.3%) | 813.6(-7.4%) |
| $\alpha_S=0.1207$ | 116.9(1.2%) | 187.9(0.4%) | 255.7(-1.2%) | 940.7(7%) |
| Total uncertainty | 4.6% | 6.4% | 17% | 14% |

TABLE IX: Theoretical uncertainty of background processes excluding the uncertainty arising from the PDF set parameters errors. The central value of cross sections has been calculated using MRST2004 NNLO PDF set with a central value of $\alpha_S = 0.1167$.

where ϵ_S is the total selection efficiency of the signal, N_S is the expected number of signal events and N_B is the contamination in the observed sample which can be derived either from real data or simulation. In the latter case, the theoretical values of the backgrounds cross sections are used together with the selection efficiencies calculated from the simulation. Measuring N_S in two different final states would allow possibility of comparing two numbers from the two final states and estimating branching ratio of ϕ^\pm decays which in turn leads to the knowledge of model parameters such as $g_{i\alpha}$.

In order to estimate the uncertainty with which N_S would be measured, the relative error on N_S is calculated as the following:

$$\frac{\Delta N_S}{N_S} = \frac{\Delta \epsilon_S}{\epsilon_S} \oplus \frac{\Delta N_{obs.}}{N_S^{sel.}} \oplus \frac{\Delta N_B}{N_S^{sel.}} \quad (24)$$

where \oplus means square root of quadratic sum of all terms. Recall that N_S is the original number of events produced at the LHC, while $N_S^{sel.}$ is the number of selected signal events at the end of selection cuts; *i.e.*, $N_S^{sel.} = \epsilon_S N_S$. The relative uncertainty of the efficiency, $\Delta \epsilon_S / \epsilon_S$, is a quadratic sum of the main uncertainties; *i.e.*, the jet energy scale uncertainty, missing transverse energy uncertainty and lepton reconstruction uncertainty. As the best guesses for achievable uncertainties in LHC detectors, an uncertainty of 3% for jet energy scale Ref. [17] and missing transverse energy and 2% for lepton reconstruction and selection are assumed at an integrated luminosity of $30 fb^{-1}$. The total selection efficiency could therefore have an uncertainty of 5% or better which is smaller than the uncertainty of the background in the sample due to the large amount of remaining background events. Suppose N_B is measured using theoretical cross section values and selection efficiencies from simulation. The uncertainty of N_B relative to signal is then

$$\frac{\Delta N_B}{N_S^{sel.}} = \left(\frac{\Delta \sigma}{\sigma} \oplus \frac{\Delta L}{L} \oplus \frac{\Delta \epsilon_B}{\epsilon_B} \right) \frac{N_B}{N_S^{sel.}} \quad (25)$$

The uncertainty of the theoretical background cross sections originates from the choice of PDF set, the PDF set parameters errors, the value of α_S used in the PDF set and the renormalization and factorization scale uncertainty. Some of these uncertainties have been estimated for the $t\bar{t}$ events in Ref. [18] and lead to a $\sim 14\%$ uncertainty for this background which should be added to the uncertainty due to the PDF fit parameters. We also study the theoretical background uncertainties independently using MCFM package (excluding the error from PDF fit parameters which needs a dedicated detailed analysis). Results are shown in Tab. IX. The renormalisation scale is set to the characteristic mass in the event, *i.e.*, the top quark, W boson and Z boson masses for $t\bar{t}$, W +jets, WW and Z +jets respectively. The variation of renormalisation scale is then performed around the central value. The central value of α_S according to PDG Ref. [19] is 0.1176 ± 0.002 . The central value of this parameter chosen by different PDF sets is different, however, the 0.002 uncertainty is interpreted as one- σ or 68% uncertainty and a 95% uncertainty ($\sim 2\sigma$) equal to 0.004 is therefore used for the α_S variation. This leads to the values of 0.1127 and 0.1207 using the central α_S value adopted by MRST2004 NNLO PDF set. The total error has been calculated as proposed in Eq. 26.

$$\text{Total error} = \sqrt{\frac{(\text{Ren. Scale } \uparrow)^2 + (\text{Ren. Scale } \downarrow)^2}{2} + (\text{max PDF set error})^2 + \frac{(\alpha_S \uparrow)^2 + (\alpha_S \downarrow)^2}{2}} \quad (26)$$

where (Ren. Scale \uparrow) and (Ren. Scale \downarrow) are the observed error on the central cross sections when the renormalisation scale is respectively set to twice and half the central value. Similarly, $(\alpha_S \uparrow)$ and $(\alpha_S \downarrow)$ are errors on central cross sections when α_S is set to respectively 0.1207 and 0.1127. For example, for the WW case, (Ren. Scale \uparrow) = -3.5 %, (Ren. Scale \downarrow) = 1.9 %, $(\alpha_S \uparrow)$ = 1.2 % and $(\alpha_S \downarrow)$ = -1 %. The middle term in Eq. (26) is the maximum uncertainty observed due to a specific PDF set. As the error due to the PDF fit parameters can be of the order of the error due to the choice of PDF or α_S variation (e.g. cf. Ref. [20]) an average total error of $\sim 10\%$ is expected for the main background processes. It should be noted that here the errors due to the top quark, W and Z boson mass measurements were neglected although they could also contribute sizably to the total error. All arguments above imply that an average 10% error on the main backgrounds is a reasonable assumption.

Taking 3% uncertainty for the LHC luminosity [21] and 10% uncertainty on background cross sections, for $m_{(\phi^\pm)} = 80$ GeV, this term is estimated to be

$$\frac{\Delta N_B}{N_S^{sel.}}(\mu\mu) \simeq 58\% . \quad (27)$$

Here only the result on the $\mu\mu$ final state has been presented as the $\tau\mu$ final state suffers from the large background contamination.

The second term on the right side of Eq. (24) refers to the ratio of statistical uncertainty of the observed number of events to the number of signal events and can be written as

$$\frac{\Delta N_{obs.}}{N_S^{sel.}} = \frac{\sqrt{N_{obs.}}}{N_S^{sel.}} . \quad (28)$$

This term amounts to 12% for the $\mu\mu$ final states. Thus, the dominant contribution to $\Delta N_S/N_S$ is the last term of Eq. (24). As far as the uncertainties in the selection of events and the collider luminosity and cross section values remain the same, the last term, which is proportional to $N_B/N_S^{sel.}$, does not change with luminosity. An improvement is therefore possible only by acquiring a better knowledge of the uncertainties involved in the analysis or increasing the center of mass energy to obtain a higher ratio of signal to background. In principle, by using the data from the LHC itself, it would be possible to reduce the uncertainties.

VI. AN ALTERNATIVE CHANNEL: THE $\phi^\pm\phi_2 + \phi^\pm\delta_2$ PRODUCTION

In this section, we study the alternative channel, $pp \rightarrow \phi^\pm\phi_2 + \phi^\pm\delta_2$. Remember that the gauge coupling of the neutral CP-odd and CP-even components of Φ (ϕ_1 and ϕ_2) to $W^\pm\phi^\mp$ are similar. On the other hand, for small values of the mixing ($\alpha \simeq 0.01$), $\delta_2 \simeq \phi_2$. From the production point of view, δ_2 therefore behaves like ϕ_2 so it is enough to study the first process (*i.e.*, $pp \rightarrow \phi^\pm\phi_2$) and double the number of events to account for the $\phi^\pm\delta_2$ production as well. In this analysis, we take $m_{\phi_2} = m_{\delta_2} = 90$ GeV in accord with Ref. [5] which imposes a lower limit of 90 GeV on the neutral Higgs boson mass. With the above assumptions, processes such as $\phi_2, \delta_2 \rightarrow \phi^\pm W^\mp$, $\phi_2 \rightarrow \delta_2 Z^0$ or $\delta_2 \rightarrow \phi_2 Z^0$ will be forbidden and $\phi_2(\delta_2)$ will have only invisible decay modes. Since ϕ_2 appears as missing energy in the detector, the final state to analyze is μE_T^{miss} or τE_T^{miss} depending on the decay of ϕ^\pm to a muon or τ . As before, we take $\text{BR}(\phi^\pm \rightarrow \mu^\pm N_1) = \text{BR}(\phi^\pm \rightarrow \tau^\pm N_1) = 0.5$.

The simulation of these events is done by considering that ϕ_2 , a CP-odd neutral scalar, would behave like A^0 in MSSM and its production process would therefore resemble the $H^\pm A^0$ production in the framework of the MSSM. Within the MSSM, the CP-odd and CP-even Higgs particles are produced similarly. Since the $H^\pm A^0$ process is not produced by PYTHIA, we use $H^\pm H^0$ to produce the signal events. The coupling of H^\pm to $W^\pm H^0$ is given by $(e^2/\sin^2 \theta_W) \sin(\beta - \alpha)$ so setting $\cos(\beta - \alpha) = 0$, the coupling will be the same as the coupling of ϕ^\pm to $W^\mp \delta_2$ within our model. Moreover, in this analysis we set $\tan(\beta) = 100$ and obtain cross sections in agreement with Ref. [22]. To produce the same type of events, in production of $H^\pm H^0$ events, H^0 is forced to decay only to a muon pair and those muons are ignored in the event to have the same lepton multiplicity as in $\phi^\pm\phi_2$ production. The missing transverse energy is also calculated by ignoring the H^0 products (muons) in the event so treating it as a source of invisible energy. Figure 14 compares E_T^{miss} as calculated only from the N_1 in ϕ^\pm decay and the total E_T^{miss} including invisible energy from ϕ_2 . Figure 15 shows the calculated total cross section of the signal for different ϕ^\pm masses. This is the inclusive cross section although there is a little difference between the production rate of ϕ^+ and ϕ^- at the LHC. Since the final state is either μE_T^{miss} or τE_T^{miss} , the main background for this signal would be single W boson production. All other backgrounds are expected to be suppressed by requirements on lepton multiplicity and central jet veto. Figures 16, 17, 18 and 19 compare the signal and background distributions of the muon transverse momentum, jet transverse

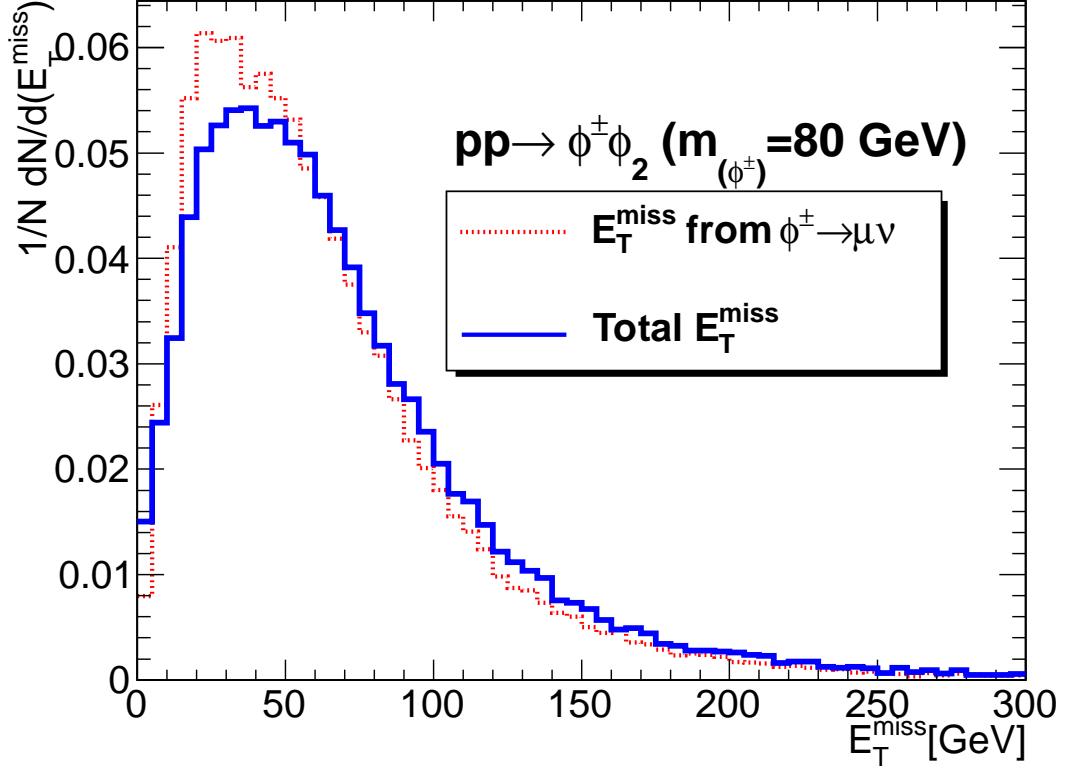


FIG. 14: Distribution of total E_T^{miss} and its comparison with distribution of E_T^{miss} from $\phi^\pm \rightarrow \mu\nu$.

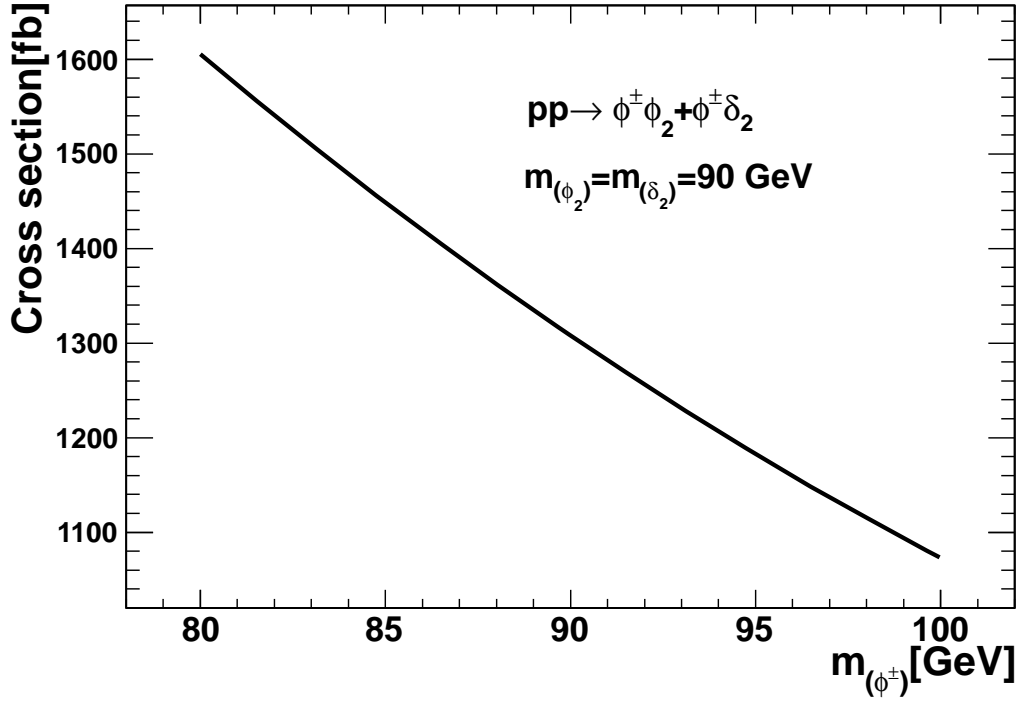


FIG. 15: Total signal cross section in the $\phi^\pm \phi_2$ channel as a function of ϕ^\pm mass.

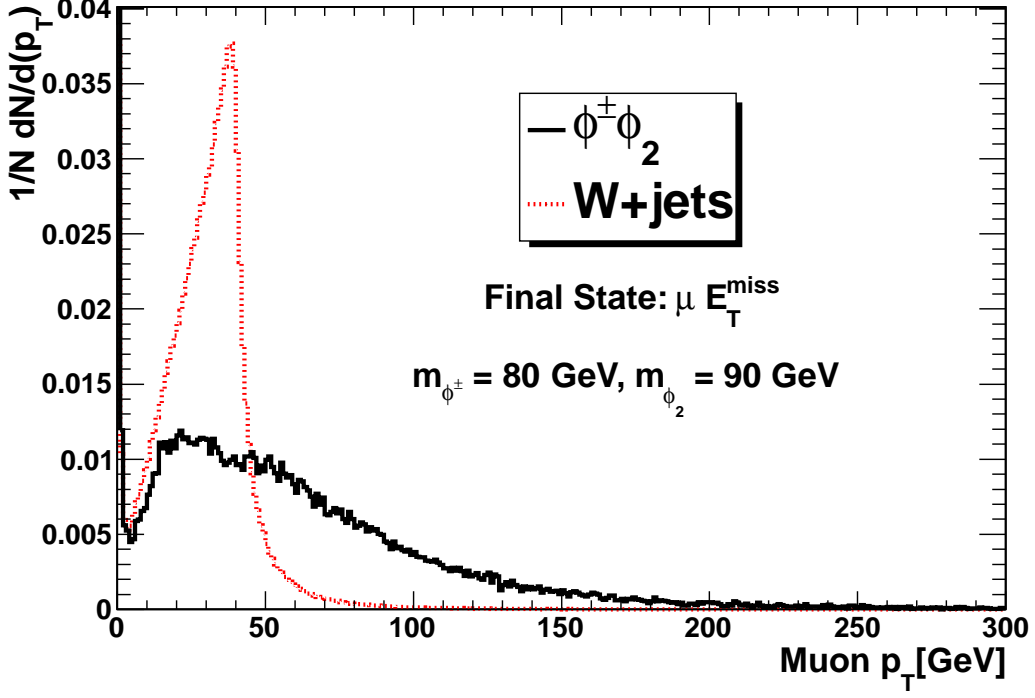


FIG. 16: Muon transverse momentum distribution in $\phi^\pm\phi_2$ events in μE_T^{miss} final state.

energy, jet multiplicity and E_T^{miss} respectively in the μE_T^{miss} final state. Based on these distributions and since the background cross section is high and needs a large suppression factor, the following kinematic cuts are applied:

$$\text{Muon } p_T > 100 \text{ GeV}, |\eta| < 2.5, \quad (29)$$

$$E_T^{\text{miss}} > 100 \text{ GeV}. \quad (30)$$

$$\text{Jet } E_T > 60 \text{ GeV}, |\eta| < 2.5. \quad (31)$$

There should be no jet in the event with μE_T^{miss} final state passing the above requirement. Similarly Figs. 20 and 21 compare the signal and background distributions of the jet transverse energy and jet multiplicity respectively in the τE_T^{miss} final state. The missing transverse energy distribution is not studied based on the same argument as mentioned in the $\tau\mu E_T^{\text{miss}}$ final state analysis of $\phi^+\phi^-$ process. For this final state the same cut on the jet E_T is applied. Since there is a τ lepton in the event, the same τ -jet identification as in the analysis of $\tau\mu E_T^{\text{miss}}$ is applied. Similarly to the $\tau\mu E_T^{\text{miss}}$ case, the polarization dependent cuts are not applied. Based on selection requirements of the two final states, Tabs. X and XI show selection efficiencies of signal and background events and the remaining number of events. Thus for $m_{(\phi^\pm)} = 80 \text{ GeV}$, a signal significance of 9σ and 4.6σ is respectively obtained for μE_T^{miss} and τE_T^{miss} final states at 30 fb^{-1} integrated luminosity. Choosing the other point in the parameter space (the point B in Table I), one obtains $BR(\phi^\pm \rightarrow e^\pm N_1) = 1/3$ so the signal cross section in the $e E_T^{\text{miss}}$ final state would be two third of that in the μE_T^{miss} final state using point A in Table I. The $e E_T^{\text{miss}}$ significance is therefore expected to be $2/3 \times 9 = 6\sigma$. Since the cross section of the signal decreases with increasing $m_{(\phi^\pm)}$, higher ϕ^\pm masses would lead to lower signal significances.

VII. DISCOVERY POTENTIAL AT THE 7 TEV RUN

In this section, an estimation of signal significance at different final states is made by a simple rescaling of the signal and background cross sections to their corresponding values at the 7 TeV center of mass energy. Although a detailed study of kinematic distributions at this energy is needed to reach a concrete conclusion, a simple cross section rescaling

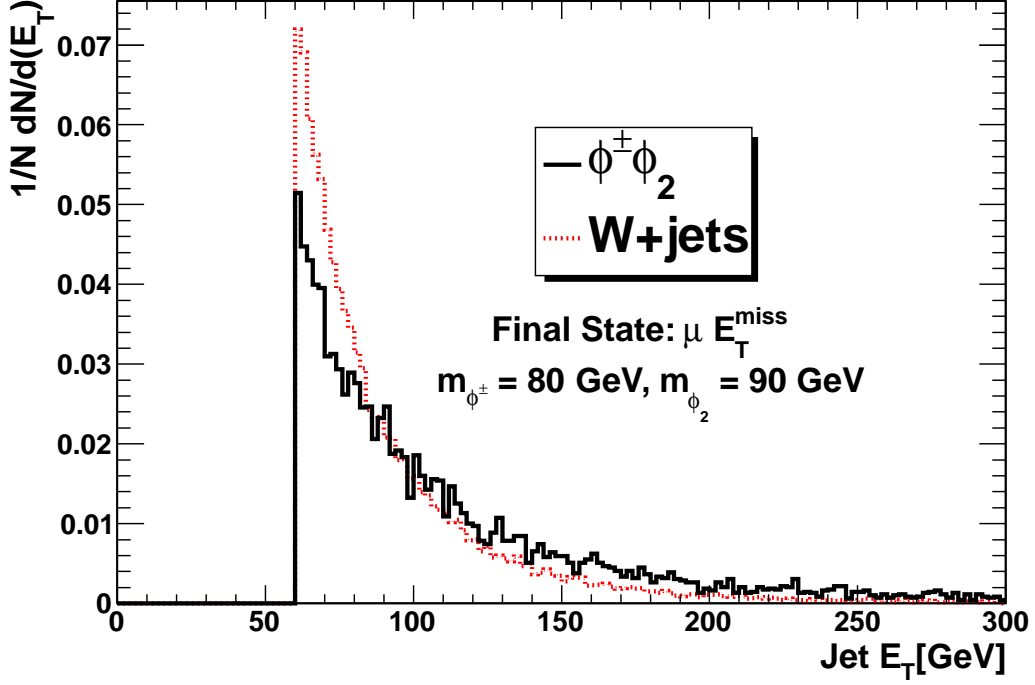


FIG. 17: Jet transverse energy distribution in $\phi^\pm \phi_2$ events in μE_T^{miss} final state. Jets satisfying Eq. 31 fill the histogram. Softer jets with $E_T < 60 \text{ GeV}$ are skipped due to the same reason explained in caption of Fig. 5.

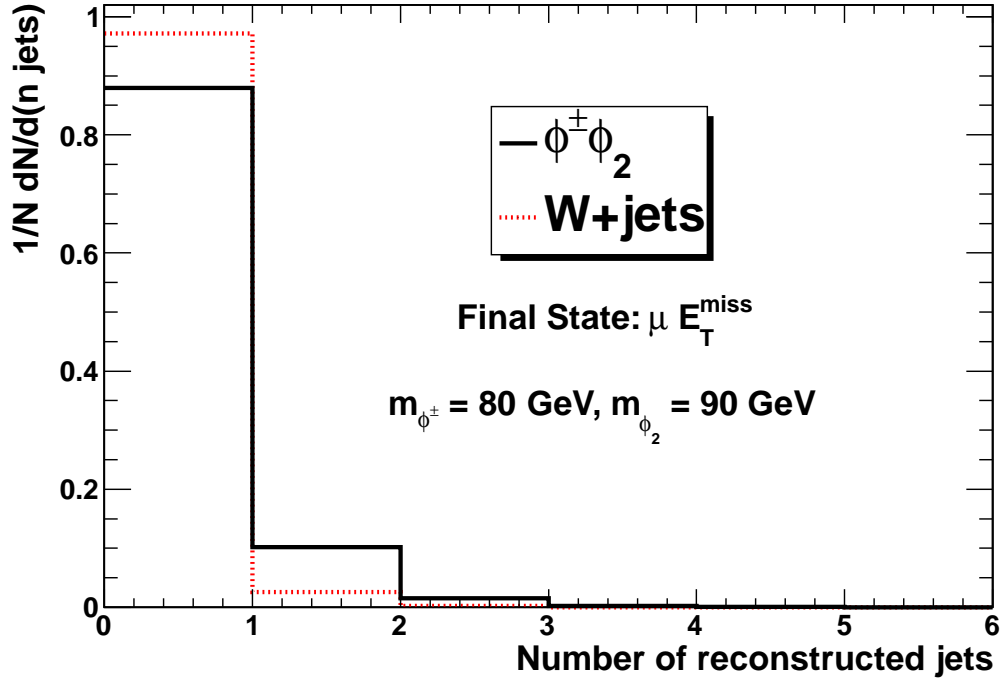


FIG. 18: Number of reconstructed jets for the $\phi^\pm \phi_2$ events in μE_T^{miss} final state. A jet is considered and counted if it passes the kinematic requirements described in the text.

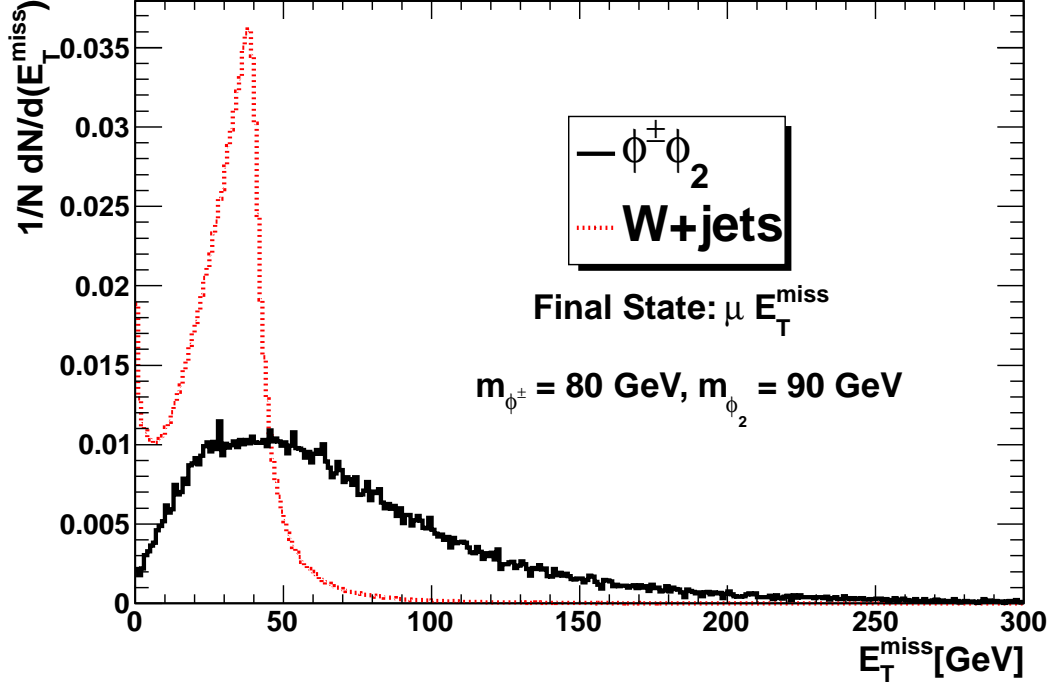


FIG. 19: Missing transverse energy distribution for the $\phi^\pm \phi_2$ events in the μE_T^{miss} final state.

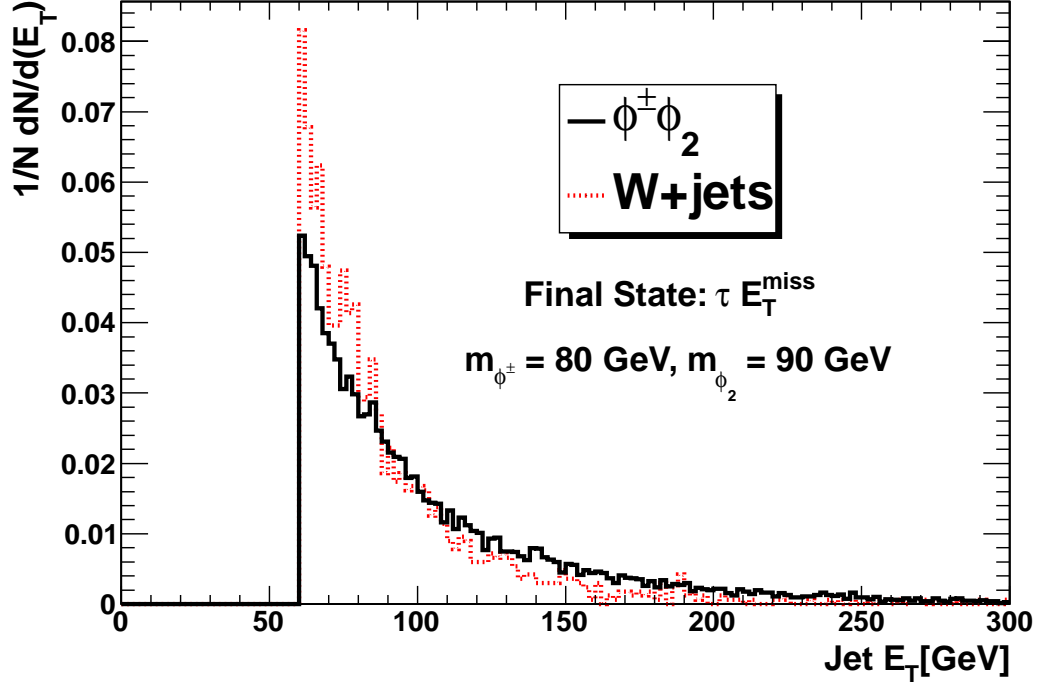


FIG. 20: Jet transverse energy distribution for the $\phi^\pm \phi_2$ events in the τE_T^{miss} final state. Here also only jets satisfying Eq. 31 fill the histogram. Softer jets with $E_T < 60 \text{ GeV}$ are skipped due to the same reason explained in caption of Fig. 5.

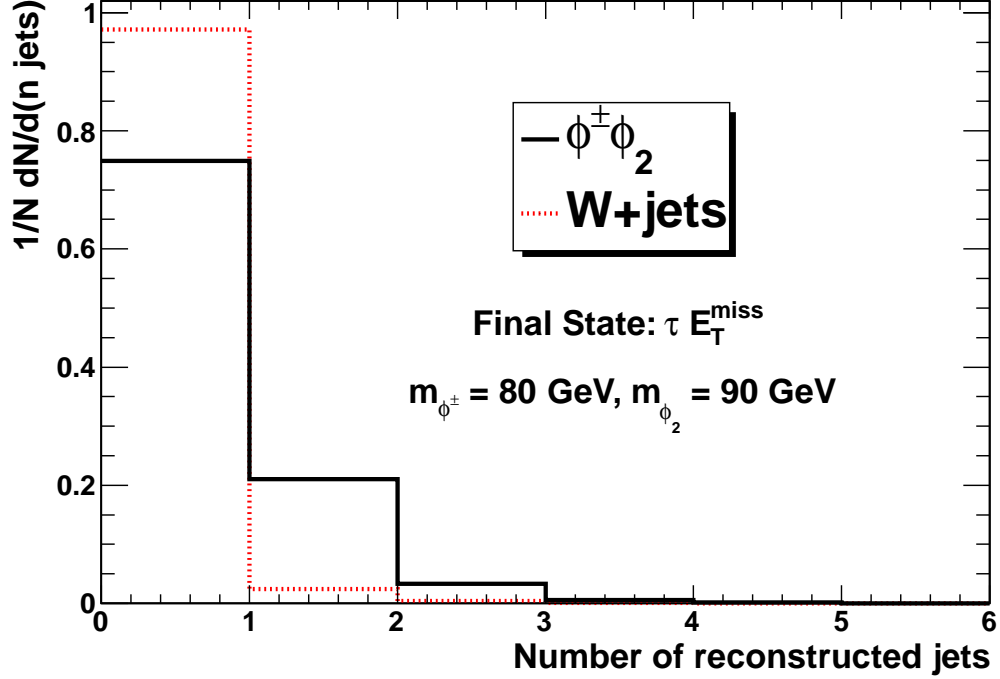


FIG. 21: Number of reconstructed jets for the $\phi^\pm\phi_2$ events in the τE_T^{miss} final state. A jet is considered and counted if it passes the kinematic requirements described in the text.

| Final state | μE_T^{miss} | |
|--|------------------|---------------------|
| Process | Signal | W+jets |
| Total cross section [pb] | 1604 | 187.3×10^3 |
| Number of events at 30 fb^{-1} | 24057 | 5.9×10^8 |
| N Muons = 1 | 3928(16%) | 1952900(0.3%) |
| N Jets = 0 | 3182(81%) | 356404(18%) |
| $E_T^{miss} > 100 \text{ GeV}$ | 2652(83%) | 87319(24%) |
| total efficiency | 11% | 0.015% |
| Expected events at 30 fb^{-1} | 2652 | 87319 |

TABLE X: Selection efficiencies and remaining number of background events after each cut in the μE_T^{miss} final state. Numbers in parentheses are relative efficiencies in percent with respect to the previous cut. Branching ratios have been taken into account in transition from the third to forth row. To calculate the signal, both $\phi^\pm\phi_2$ and $\phi^\pm\delta_2$ have been taken into account.

would give first feeling on how signal significance would decrease at lower center of mass energies. We choose the 7 TeV center of mass energy to discuss the possibility of establishing the model introduced in this paper at the current LHC run. Table XII shows ratio of 7 TeV to 14 TeV cross section of signal and background processes. These ratios lead to the signal significance as shown in Table XIII for different final states, provided that the data corresponding to 30 fb^{-1} integrated luminosity is collected at the 7 TeV center of mass energy. This assumption might be in contrast to the current plan of the LHC machine, as there may be a switch to higher center of mass energies (10 TeV and 14 TeV later on) before this amount of data is collected. If this phase finishes after collecting only 1 fb^{-1} , the expected signal significance will be $1/\sqrt{30} \simeq 0.18$ times smaller so there will be no discovery chance. However with 30 fb^{-1} , as seen from Table XIII, searching for the $\phi^+\phi^-$ process, a 5σ discovery for the $\mu\mu E_T^{miss}$ final state for ϕ^\pm masses below $\sim 100 \text{ GeV}$ will be possible. A discovery for μE_T^{miss} final state of $\phi^\pm\phi_2 + \phi^\pm\delta_2$ is also possible for $m_{(\phi^\pm)} = 80 \text{ GeV}$. The needed integrated luminosity for this conclusion is 30 fb^{-1} .

| Final state | τE_T^{miss} | |
|--|-------------------|--------------------------|
| Process | Signal | W+jets |
| Total cross section [pb] | 1604 | 187.3×10^3 |
| Number of events at 30 fb^{-1} | 24057 | 5.9×10^8 |
| N Jets = 1 | 5117(21.3%) | 1.5×10^7 (2.6%) |
| Isolation | 3058(59.8%) | 1.2×10^6 (7.7%) |
| 1- or 3-prong decay | 2900(94.8%) | 389380(33%) |
| total efficiency | 12.05% | 0.066% |
| Expected events at 30 fb^{-1} | 2900 | 389380 |

TABLE XI: Selection efficiencies and remaining number of background events after each cut in the τE_T^{miss} final state. Numbers in parentheses are relative efficiencies in percent with respect to the previous cut. Branching ratios have been taken into account in transition from the third to forth row. To calculate the signal, both $\phi^\pm \phi_2$ and $\phi^\pm \delta_2$ have been taken into account.

| Signal | | |
|-------------------|------------------------------------|-----------------------|
| Channel | Mass Point | 7 TeV to 14 TeV Ratio |
| $\phi^+ \phi^-$ | $m_{(\phi^\pm)} = 80 \text{ GeV}$ | 0.4 |
| | $m_{(\phi^\pm)} = 90 \text{ GeV}$ | 0.39 |
| | $m_{(\phi^\pm)} = 110 \text{ GeV}$ | 0.37 |
| | $m_{(\phi^\pm)} = 130 \text{ GeV}$ | 0.35 |
| $\phi^\pm \phi_2$ | $m_{(\phi^\pm)} = 80 \text{ GeV}$ | 0.4 |
| Background | | |
| Channel | 7 TeV to 14 TeV Ratio | |
| $W^+ W^-$ | 0.38 | |
| $t\bar{t}$ | 0.19 | |
| W+jets | 0.49 | |
| Z+jets | 0.6 | |

TABLE XII: Ratio of 7 TeV to 14 TeV cross sections of signal and background events.

VIII. CONCLUSIONS

In this paper, the possibility of discovering the SLIM model proposed in [3] has been discussed. The focus has been on search for a signal at the LHC in two different categories based on the $\phi^+ \phi^-$ and $\phi^\pm \phi_2 + \phi^\pm \delta_2$ production processes. In the first category, two final states of $\tau \mu$ and $\mu \mu$ plus missing transverse energy have been analyzed in detail. The main background processes have been identified and a cut based search has been performed for the two final states separately. The search focused on 30 fb^{-1} integrated luminosity at LHC. It has been shown that the $\tau \mu$ and $\mu \mu$ final states would have a signal significance of 2.8σ and 9.2σ respectively for $m_{(\phi^\pm)} = 80 \text{ GeV}$. The ee final state has been estimated to have a significance of 4.1σ based on a simple rescaling of the $\mu \mu$ final state results. The above search allows to have a signal significance exceeding 5σ in the $\mu \mu$ final state for the ϕ^\pm masses below 130 GeV at 30 fb^{-1} . In the second category, two final states of τE_T^{miss} and μE_T^{miss} were analyzed in detail. Results indicate that a significance of 4.6σ and 9.8σ can be obtained for the above final states respectively. The $e E_T^{miss}$ final state is expected to have a significance of 6.5σ . A simple rescaling of the cross sections to their values at 7 TeV run of LHC shows that a discovery chance exists for $\mu \mu E_T^{miss}$ final state of $\phi^+ \phi^-$ and also for μE_T^{miss} final state of $\phi^+ \phi_2$ even at this center of mass energy, provided that data corresponding to 30 fb^{-1} integrated luminosity is collected before switching to higher machine energies. While the signal is observable at LHC, because of the uncertainties in the background estimation, measuring the new couplings of the model is more challenging. To make such a measurement a possibility, either these uncertainties have to be reduced or a future collider with a higher center of mass energy has to be employed.

Apart from the signals that we have discussed in the paper ($\phi^+ \phi^-$, $\phi^\pm \phi_2$ and $\phi^\pm \delta_2$), the model can have other observable effects such as the $\delta_2 \phi_2$ production or invisible Higgs decay $H \rightarrow \delta_1 \delta_1$ [3]. Studying the prospect of detecting all these modes is beyond the scope of the present paper and will be presented elsewhere.

| Channel | Mass Point | Signal significance |
|---|------------------------------------|---------------------|
| $\phi^+ \phi^- \rightarrow \tau \mu E_T^{miss}$ | $m_{(\phi^\pm)} = 80 \text{ GeV}$ | 1.6 |
| | $m_{(\phi^\pm)} = 90 \text{ GeV}$ | 1.2 |
| | $m_{(\phi^\pm)} = 110 \text{ GeV}$ | 0.7 |
| | $m_{(\phi^\pm)} = 130 \text{ GeV}$ | 0.5 |
| $\phi^+ \phi^- \rightarrow \mu \mu E_T^{miss}$ | $m_{(\phi^\pm)} = 80 \text{ GeV}$ | 6.4 |
| | $m_{(\phi^\pm)} = 90 \text{ GeV}$ | 5.7 |
| | $m_{(\phi^\pm)} = 110 \text{ GeV}$ | 4.2 |
| | $m_{(\phi^\pm)} = 130 \text{ GeV}$ | 3.0 |
| $\phi^\pm \phi_2 \rightarrow \tau E_T^{miss}$ | $m_{(\phi^\pm)} = 80 \text{ GeV}$ | 2.6 |
| $\phi^\pm \phi_2 \rightarrow \mu E_T^{miss}$ | $m_{(\phi^\pm)} = 80 \text{ GeV}$ | 5.0 |

TABLE XIII: Signal significance in different final states for the 7 TeV run, provided that 30 fb^{-1} data is collected at this energy before any switch to higher machine energies.

Appendix A

In this appendix, we derive constraints on the coupling $g_{i\alpha}$ from the neutrino mass matrix for the most economic case with only two right-handed neutrinos. As discussed in the text, in this case neutrino mass scheme is hierarchical.

- *Normal Hierarchical scheme:*

$$(m_\nu)_{\alpha\beta} = U_{PMNS} \cdot \text{Diag}[0, \sqrt{\Delta m_{sun}^2}, \sqrt{\Delta m_{atm}^2} e^{i\xi}] \cdot U_{PMNS}^T$$

where U_{PMNS} is the neutrino mixing matrix whose elements are known up to the subleading θ_{13} effects. However, we do not know the value of the Majorana phase ξ .

Using Eq. (7), we find that

$$g_{i\alpha} = \sum_j \frac{1}{A_i} (O^T \cdot \text{Diag}[(\Delta m_{sun}^2)^{1/4}, e^{i\xi/2}(\Delta m_{atm}^2)^{1/4}])_{ij} (U_{PMNS})_{\alpha j+1}, \quad (\text{A1})$$

where O is an arbitrary orthogonal matrix: $O^T \cdot O = 1$ so

$$O = \begin{bmatrix} \cos \theta & \sin \theta \\ -\sin \theta & \cos \theta \end{bmatrix}. \quad (\text{A2})$$

In this case, we do not have any prediction for the coupling ratios independent of the arbitrary θ .

- *Inverted Hierarchical scheme:*

$$(m_\nu)_{\alpha\beta} = U_{PMNS} \cdot \text{Diag}[\sqrt{\Delta m_{atm}^2}, \sqrt{\Delta m_{atm}^2 + \Delta m_{sun}^2} e^{i\xi}, 0] \cdot U_{PMNS}^T.$$

From Eq. (7), we therefore find

$$g_{i\alpha} = \sum_j \frac{1}{A_i} (O^T \cdot \text{Diag}[(\Delta m_{atm}^2)^{1/4}, e^{i\xi/2}(\Delta m_{atm}^2 + \Delta m_{sun}^2)^{1/4}])_{ij} (U_{PMNS})_{\alpha j},$$

where again O is an arbitrary orthogonal matrix as in Eq. A2. It is noteworthy that regardless of the values θ and ξ ,

$$\frac{|g_{1\tau}|^2}{|g_{1\mu}|^2} \simeq \frac{|g_{2\tau}|^2}{|g_{2\mu}|^2} \simeq 1 + O(\theta_{13}, \theta_{23} - \pi/4). \quad (\text{A3})$$

However the values of $|g_{1e}|^2/|g_{1\tau}|^2$ or $|g_{2e}|^2/|g_{2\tau}|^2$ depend on the unknown θ and ξ .

-
- [1] C. Boehm, Y. Farzan, T. Hambye, S. Palomares-Ruiz and S. Pascoli, Phys. Rev. D **77**, 043516 (2008) [arXiv:hep-ph/0612228].
 - [2] Y. Farzan, Mod. Phys. Lett. A, Vol. 25, No. 25 (2010) pp. 2111-2120.
 - [3] Y. Farzan, Phys. Rev. D **80**, 073009 (2009) [arXiv:0908.3729 [hep-ph]].
 - [4] [LEP Higgs Working Group for Higgs boson searches and ALEPH Collaboration an], arXiv:hep-ex/0107031; G. Abbiendi *et al.* [OPAL Collaboration], Eur. Phys. J. C **32** (2004) 453 [arXiv:hep-ex/0309014]; G. Abbiendi *et al.* [OPAL Collaboration], arXiv:0812.0267 [hep-ex].
 - [5] http://lephiggs.web.cern.ch/LEPHIGGS/papers/July2005_MSSM/LHWG-Note-2005-01.pdf.
 - [6] V. I. Kuvshinov, V. I. Kashkan and R. G. Shulyakovsky, arXiv:hep-ph/0107031.
 - [7] CMS Physics Technical Design Report, volume I, CERN/LHCC 2006-001, section 12.1.2
 - [8] Brief Introduction to PYTHIA 8.1, T. Sjostrand, S. Mrenna and P. Z. Skands, Comput. Phys. Commun. **178**, 852 (2008) [arXiv:0710.3820 [hep-ph]].
 - [9] S. Jadach, Z. Was, R. Decker, J.H. Kühn, Comp. Phys. Comm. 76 (1993) 361, M. Jezabek, Z. Was, S. Jadach, J.H. Kühn, Comp. Phys. Comm. 70 (1992) 69, S. Jadach, J.H. Kühn, Z. Was, Comp. Phys. Comm. 64 (1990) 275.
 - [10] N. Davidson, G. Nanava, T. Przedzinski, E. Richter-Was and Z. Was, arXiv:1002.0543 [hep-ph].
 - [11] <http://lcgapp.cern.ch/project/simu/HepMC/>.
 - [12] M. Cacciari and G. P. Salam, Phys. Lett. B **641**, 57 (2006) [arXiv:hep-ph/0512210].
 - [13] M. Cacciari, G. P. Salam and G. Soyez, JHEP **0804**, 063 (2008) [arXiv:0802.1189 [hep-ph]].
 - [14] <http://mcfm.fnal.gov/>.
 - [15] <http://projects.hepforge.org/lhapdf/>.
 - [16] <http://pdg.lbl.gov/>.
 - [17] CMS Physics Technical Design Report, volume I, CERN/LHCC 2006-001, section 11.6.5.
 - [18] Top Quark Physics, A. Ahmadov, et al., <http://arxiv.org/pdf/hep-ph/0003033v1>, Section 3.2
 - [19] <http://pdg.lbl.gov/2009/reviews/rpp2009-rev-phys-constants.pdf>
 - [20] M. Ubiali, R. D. Ball, L. Del Debbio, S. Forte, A. Guffanti, J. I. Latorre and J. Rojo, arXiv:1005.0397 [hep-ph].
 - [21] CMS Physics Technical Design Report, volume I, CERN/LHCC 2006-001, section 8.1.2, CMS Physics Technical Design Report, volume II, CERN/LHCC 2006-021, section B.2.1.
 - [22] Q. H. Cao, S. Kanemura and C. P. Yuan, Phys. Rev. D **69**, 075008 (2004) [arXiv:hep-ph/0311083] and references therein.